Article

SOURCE DATA | TRANSPARENT PROCESS

THE EMBO JOURNAL

Distinct *in vivo* roles of secreted APP ectodomain variants APPsα and APPsβ in regulation of spine density, synaptic plasticity, and cognition

Max C Richter[1,†], Susann Ludewig[2,†], Alex Winschel[3], Tobias Abel[4], Charlotte Bold[1], Leonie R Salzburger[2], Susanne Klein[1], Kang Han[1], Sascha W Weyer[1], Ann-Kristina Fritz[5,6], Bodo Laube[3], David P Wolfer[5,6], Christian J Buchholz[4], Martin Korte[2,7] & Ulrike C Müller[1,*]

Abstract

Increasing evidence suggests that synaptic functions of the amyloid precursor protein (APP), which is key to Alzheimer pathogenesis, may be carried out by its secreted ectodomain (APPs). The specific roles of APPsα and APPsβ fragments, generated by non-amyloidogenic or amyloidogenic APP processing, respectively, remain however unclear. Here, we expressed APPsα or APPsβ in the adult brain of conditional double knockout mice (cDKO) lacking APP and the related APLP2. APPsα efficiently rescued deficits in spine density, synaptic plasticity (LTP and PPF), and spatial reference memory of cDKO mice. In contrast, APPsβ failed to show any detectable effects on synaptic plasticity and spine density. The C-terminal 16 amino acids of APPsα (lacking in APPsβ) proved sufficient to facilitate LTP in a mechanism that depends on functional nicotinic α7-nAChRs. Further, APPsα showed high-affinity, allosteric potentiation of heterologously expressed α7-nAChRs in oocytes. Collectively, we identified α7-nAChRs as a crucial physiological receptor specific for APPsα and show distinct *in vivo* roles for APPsα versus APPsβ. This implies that reduced levels of APPsα that might occur during Alzheimer pathogenesis cannot be compensated by APPsβ.

Keywords Alzheimer; amyloid precursor protein; nicotinic acetylcholine receptor; soluble APPsα; synaptic plasticity

Subject Categories Neuroscience

DOI 10.15252/embj.201798335 | Received 29 September 2017 | Revised 23 February 2018 | Accepted 2 March 2018 | Published online 16 April 2018

The EMBO Journal (2018) 37: e98335

Introduction

Alzheimer's disease (AD) is characterized by the accumulation of β-amyloid peptides (Aβ) that are derived from the amyloid precursor protein (APP) by proteolytic cleavage (Selkoe & Hardy, 2016). Two principal physiological pathways either prevent or promote Aβ generation. Within the amyloidogenic pathway, APP processing is shifted towards the production of Aβ and secreted APPsβ, by consecutive β-secretase (BACE1) and γ-secretase cleavage (Vassar *et al*, 2014). In AD, BACE1 is upregulated, favoring amyloidogenic APP processing (Holsinger *et al*, 2002; Ahmed *et al*, 2010). In the alternative, non-amyloidogenic pathway cleavage of APP within the Aβ region by the major α-secretase ADAM10 (a disintegrin and metalloprotease) prevents Aβ generation and liberates APPsα that is secreted into the extracellular space (Saftig & Lichtenthaler, 2015). Shifting APP processing towards non-amyloidogenic processing has therefore been suggested as a therapeutic strategy for AD (Mockett *et al*, 2017). An important and still unresolved question is whether in addition to neurotoxic Aβ accumulation a concomitant reduction in APPsα level, or an altered APPsα/APPsβ ratio may contribute to AD symptoms and pathogenesis (reviewed by Mockett *et al*, 2017). In this regard, it will be crucial to know whether APPsα and APPsβ, that is only 16 amino acids shorter than APPsα, serve largely similar or distinct, possibly even opposite physiological functions. While our previous studies and work from others indicated that APPsα has neurotrophic and neuroprotective effects, including synaptogenic, LTP facilitating and memory enhancing properties (Meziane *et al*, 1998; Ring *et al*, 2007; Taylor *et al*, 2008; Milosch *et al*, 2014; Weyer *et al*, 2014; Hick *et al*, 2015; Hefter *et al*, 2016; Plummer *et al*, 2016), only few and mostly conflicting studies have as yet addressed the functions of APPsβ (Nikolaev *et al*, 2009; Li *et al*, 2010; Weyer *et al*, 2011; Chasseigneaux & Allinquant, 2012). So far,

1 Institute of Pharmacy and Molecular Biotechnology (IPMB), Ruprecht-Karls University Heidelberg, Heidelberg, Germany
2 Zoological Institute, Division of Cellular Neurobiology, TU Braunschweig, Braunschweig, Germany
3 Department of Biology, Neurophysiology und Neurosensory Systems, TU Darmstadt, Darmstadt, Germany
4 Paul-Ehrlich-Institut (PEI), Langen, Germany
5 Institute of Anatomy, University of Zurich, Zurich, Switzerland
6 Institute of Human Movements Sciences and Sport, ETH Zurich, Zurich, Switzerland
7 Helmholtz Centre for Infection Research, AG NIND, Braunschweig, Germany
*Corresponding author. Tel: +49 6221 546717; E-mail: u.mueller@urz.uni-heidelberg.de
†These authors contributed equally to this work

the molecular basis of any difference compared to APPsα remained unclear. Thus, a more detailed knowledge about the specific functions of the secreted APP ectodomains is essential to understand AD pathogenesis and evaluate risks of ongoing pharmacotherapy, as well as to elucidate APP physiology.

There is a large body of evidence indicating that APP family proteins are multimodal proteins that can function as ligands via their secreted fragments or as cell surface proteins important for synaptic adhesion and signal transduction (Müller *et al*, 2017). Major insights into the physiological functions of APP and the related APLPs (APP like proteins) were obtained from knockout models (Müller *et al*, 2017). While most impairments of APP-KO mice emerged only in aged mice (Dawson *et al*, 1999; Seabrook *et al*, 1999; Ring *et al*, 2007; Lee *et al*, 2010; Tyan *et al*, 2012), combined APP/APLP2 double knockout mice die shortly after birth, likely due to severe deficits at the neuromuscular junction (von Koch *et al*, 1997; Heber *et al*, 2000; Wang *et al*, 2005; Klevanski *et al*, 2014). Recently generated forebrain-specific double knockout mice (termed NexCre cDKO), that lack APP from embryonic day 11.5 onwards in excitatory forebrain neurons on a global constitutive APLP2-KO background, showed a severe synaptic phenotype already at young age, including reduced spine density and impaired LTP in the hippocampus, as well as deficits in learning and memory (Hick *et al*, 2015). Interestingly, the LTP impairment of NexCre cDKO mice could be ameliorated by acute APPsα application onto brain slices *in vitro*, while the molecular mechanism and receptor(s) mediating its function remained unknown (Hick *et al*, 2015).

More recently, we showed that AAV-mediated intracranial expression of APPsα can mitigate the Aβ-related synaptic deficits of APP/PS1 mice *in vivo* (Fol *et al*, 2016). Intracranial AAV-APPsα injections enhanced spine density, improved LTP deficits and memory, but at the same time also reduced soluble Aβ levels and plaque load, likely due to enhanced Aβ clearance (Fol *et al*, 2016). In addition, APPsα had been reported to lower Aβ by directly binding to and inhibiting BACE (Obregon *et al*, 2012). These results raised the question of whether the beneficial *in vivo* effects of APPsα are mainly due to its Aβ lowering properties.

Here, we asked whether APPsα may also have synaptotrophic effects in an Aβ-independent pathology with synaptic impairments and used viral vectors to express APPsα intracranially in NexCre cDKO mice. Moreover, we set out to compare side by side the properties of APPsα and APPsβ *in vivo*. We demonstrate that APPsα is sufficient to fully rescue hippocampal spine density, to restore LTP and partially rescue spatial memory in adult NexCre cDKO mice. In sharp contrast, despite similar expression level, APPsβ failed to show any detectable effects on synaptic plasticity and spine density. Finally, we show that the CTα16 domain of APPsα (that is lacking in APPsβ) is able to facilitate LTP to the same extent as APPsα, in a mechanism that involves functional nicotinic α7 acetylcholine receptors (α7-nAChRs). Moreover, we show that nanomolar concentrations of APPsα (but not APPsβ) can directly potentiate α7-nAChRs-mediated currents upon heterologous expression in *Xenopus* oocytes and increases the apparent agonist affinity as a positive allosteric modulator. Collectively, our analysis identifies the α7-nAChR as a crucial physiological receptor for APPsα and reveals distinct *in vivo* roles of APPsα vs. APPsβ.

Results

AAV-APPsα injection mediates efficient and neuron-specific expression of APPsα in the hippocampus of cDKO mice

To investigate whether APPsα is able to rescue the synaptic deficits of NexCre cDKO (further referred to as cDKO) animals *in vivo*, APPsα was expressed in the adult brain using stereotactic injection. We employed an AAV9-based bicistronic vector (AAV-APPsα; Fig 1A) coding for Venus and codon-optimized HA-tagged murine HA-APPsα that was inserted behind the APP signal peptide (SP). The HA-APPsα reading frame was fused to Venus by a T2A site to enable tracking of transduced cells. Expression was driven by the neuronal synapsin promoter. Monocistronic AAV-Venus vector served as a control (AAV-Venus; Fig 1A). Adult cDKO animals (aged 4–5 months) were either injected with AAV-APPsα or AAV-Venus control vector, whereas littermate control mice (LM control) received only AAV-Venus. Thus, comparison of AAV-Venus-injected cDKO mice with AAV-Venus-injected LM controls was expected to yield similar synaptic impairments as previously observed for uninjected cDKO mice (Hick *et al*, 2015). Vectors were bilaterally injected (dose: 1.0×10^9 gc/μl per injection spot) into the stratum lacunosum-moleculare region of the dorsal hippocampus and into the dentate gyrus (Fig 1B). To evaluate Venus and APPsα expression, animals were sacrificed 6 weeks post-injection and brain samples were analyzed by Western blot and immunohistochemistry using an HA-tag-specific antibody. Analysis of serial anteroposterior coronal brain sections (Bregma −1.10 to Bregma −2.70; see Fig EV1C) revealed widespread expression of APPsα in the hippocampus and, to a considerably lower extent, also in adjacent cortical areas (Figs 1C and EV1C). Along the longitudinal (dorsal-ventral) axis of the hippocampus, APPsα expression was much more pronounced in the dorsal region, whereas expression was not detectable in the ventral hippocampus (Fig EV1C).

As Venus contained a membrane anchor, we observed prominent accumulation in dendritic regions, whereas HA-APPsα staining was intense in intracellular membrane compartments consistent with the transport of APPsα within the secretory pathway to the cell surface for secretion (see also Fig EV2D and E for co-localization with ER and Golgi markers). In the CA3 region, APPsα expression appeared slightly lower compared to the expression obtained in pyramidal cells of the subiculum, the CA1 (Fig 1C) and the CA2 regions. Consistent with previous studies (Jackson *et al*, 2016), we noted that APPsα was detectable in HEK cells transfected with synapsin promoter driven AAV constructs (see Fig EV2A), likely due to AAV plasmid overload. *In vivo*, however, AAV-APPsα expression was restricted to neurons, as shown by double immunofluorescence staining against the HA-tag and the neuronal marker NeuN (Fig 1D and E). Consistently, no overlapping expression pattern was detectable in astrocytes (GFAP; Fig 1F) and microglia (Iba1; Fig 1G). The AAV-Venus expression pattern obtained from injections of control vector was largely similar to that of AAV-APPsα (Fig EV1C). Western blot analysis of hippocampal homogenates, using the M3.2 antibody, confirmed efficient AAV-mediated APPsα expression in injected animals (Fig 1H). Note that antibody M3.2 is directed against an epitope located between the α- and β-secretase site and recognizes endogenous APP species (APP full length and APPsα) that are still expressed by interneurons and glia in cDKO mice (see

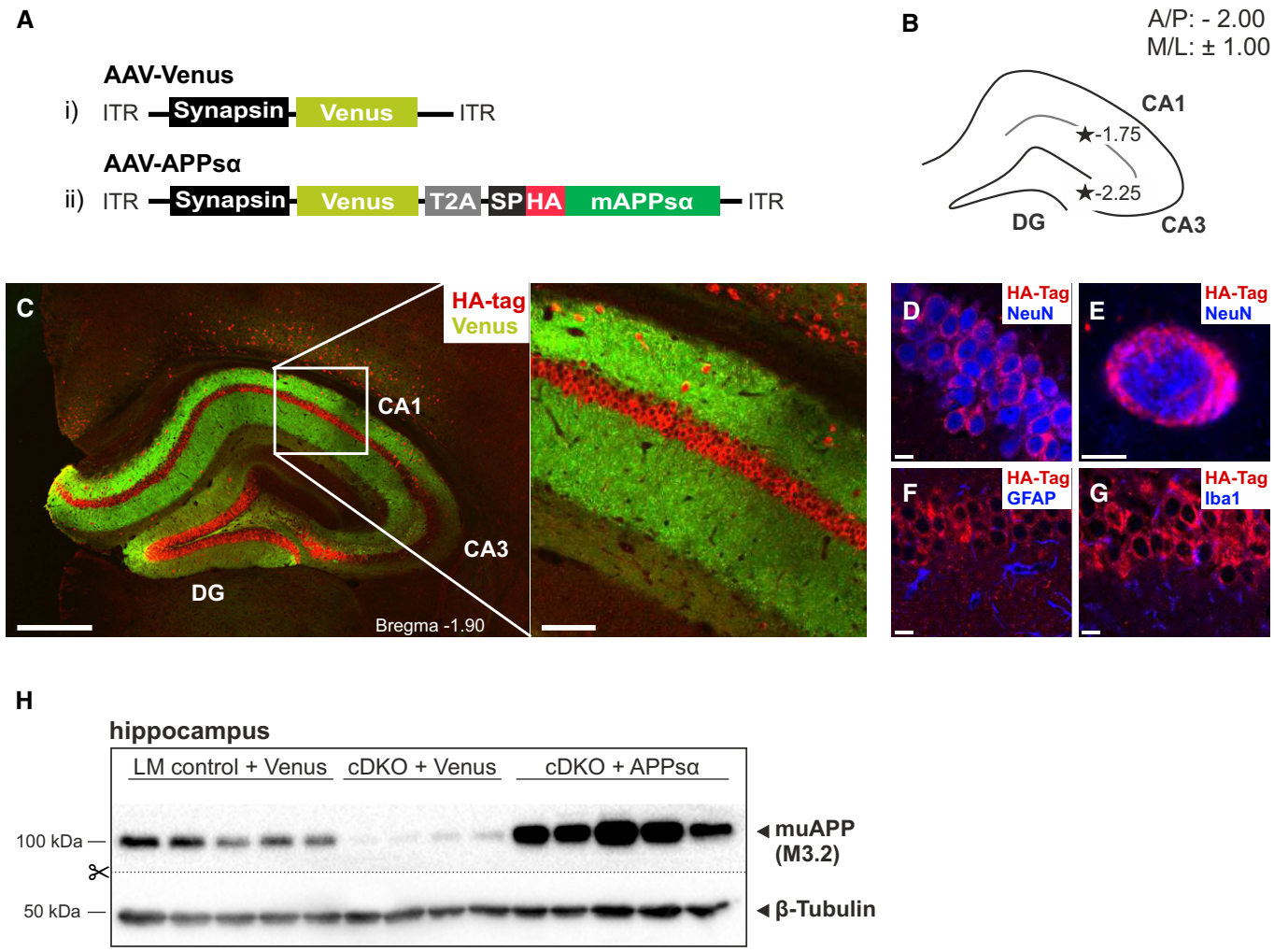

Figure 1. Expression of APPsα in the hippocampus of AAV-APPsα-injected cDKO animals.

A Schematic representation of monocistronic and bicistronic AAV constructs enabling neuron-specific expression of (i) Venus and (ii) HA-tagged APPsα (+Venus). ITR: inverted terminal repeat, Synapsin: neuron-specific promotor, T2A: *Thoseaasigna* virus 2A site, SP: signal peptide, HA: influenza hemagglutinin tag.

B Scheme of the hippocampus with coordinates of the two injection sites (black stars).

C Overview of the hippocampus of an AAV-APPsα-injected cDKO mouse. HA-tag staining (red) reveals APPsα expression within the CA1, CA3, and DG of the hippocampus. Magnification shows the boxed CA1 region. Scale bars: 500 μm (left), 100 μm (right). DG: Dentate Gyrus, CA: Cornu Ammonis.

D–G Double immunostaining in CA1 region. APPsα (HA-tag, red) is exclusively expressed in neurons (NeuN, blue, D, E), but not in astrocytes (GFAP, blue, F) or microglia (Iba1, blue, G). Scale bars: 10 μm (D, F, G), 5 μm (E).

H Western blot analysis of APP expression in hippocampus of LM control (N = 5) and cDKO mice (N = 4) injected with AAV-Venus or AAV-APPsα (N = 5). Age of mice: 5–6 months.

Source data are available online for this figure.

Hick *et al*, 2015) and vector-derived AAV-APPsα. Collectively, our data demonstrate that AAV-APPsα injection results in efficient and neuron-specific expression of APPsα throughout the dorsal hippocampus.

Impaired synaptic plasticity and reduced spine density of APP/APLP2 cDKO mice are rescued by APPsα expression in the adult brain

Having demonstrated that HA-APPsα is efficiently expressed in the hippocampus of injected animals, we evaluated whether APPsα is sufficient to rescue impairments in functional network activity that were previously reported for cDKO mice (Hick *et al*, 2015). After 20 min of baseline recording, we induced long-term potentiation (LTP) at the Schaffer collateral to CA1 pathway by application of theta burst stimulation (TBS) in acute hippocampal slices of mice that had been injected with viral vectors 6 weeks earlier (at 4–5 months of age). Consistent with our previous results (Hick *et al*, 2015), AAV-Venus-injected cDKO mice exhibited significantly lower induction and maintenance of LTP (n = 25 slices), as compared to AAV-Venus-injected LM controls (n = 23; Fig 2A). AAV-Venus-injected LM control mice

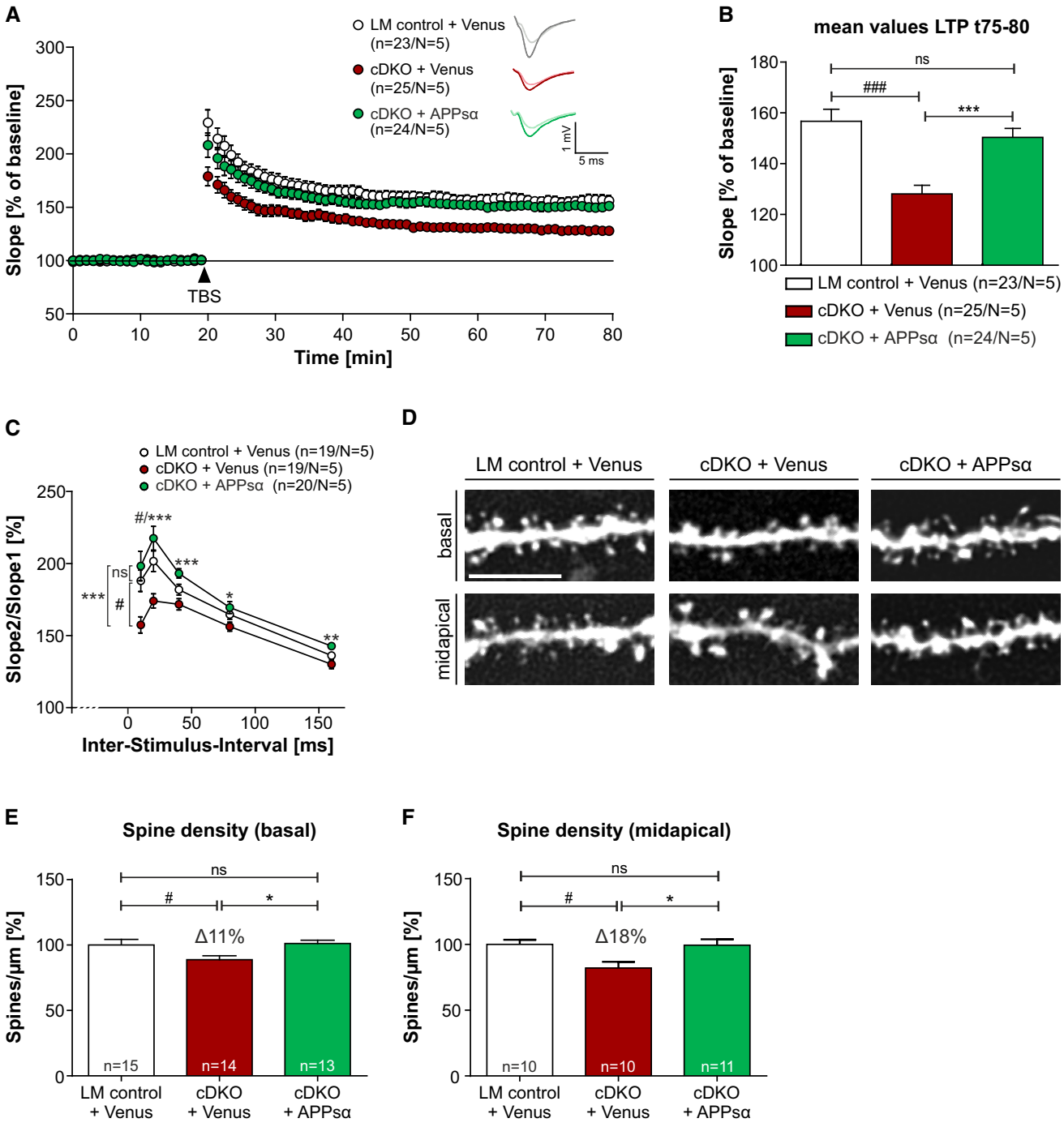

Figure 2. AAV-APPsα rescues LTP, impaired short-term synaptic plasticity, and spine density of cDKO mice.

A, B LTP was induced at hippocampal CA3-CA1 synapses after 20 min baseline recordings (arrowhead, TBS). cDKO mice expressing Venus (red) exhibited significant lower induction and maintenance of LTP (128.12 ± 3.41%) compared to Venus-injected LM controls (white, 156.69 ± 4.75%, $^{\#\#\#}P < 0.001$). AAV-mediated expression of APPsα (green) restored potentiation after start of baseline recording and resulted in a LTP curve comparable to that of LM controls. The LTP induction rate is shown as percentage % of mean baseline slope. Data points were averaged over six time points. *n* = number of slices. *N* = number of animals.

C The deficit of PPF in Venus-injected cDKO mice at the 10 ms ($^{\#}P < 0.05$) and 20 ms ($^{\#}P < 0.05$) ISI was restored by expression of APPsα. *n* = number of slices. *N* = number of animals.

D Representative images of basal and midapical dendritic segments of CA1 neurons. Scale bar: 5 µm.

E, F The spine density deficit of Venus-injected cDKOs mice (11% in basal and 18% in midapical dendrites) is rescued by APPsα to LM control levels. Images are maximum projections of deconvolved *z*-stacks. Spine density was normalized to LM control levels. *n* = number of neurons (from five animals per condition).

Data information: Age of mice at analysis: 5–6 months. Data represent mean ± SEM. Data were analyzed by one-way ANOVA followed by Bonferroni's *post hoc* test. # indicates significant differences between LM control and cDKO injected with AAV-Venus, * between cDKO injected with AAV-Venus or APPsα. $^{ns}P > 0.05$, $^{*/\#}P < 0.05$, $^{**}P < 0.01$, $^{***/\#\#\#}P < 0.001$.

showed a potentiation of 156.69 ± 4.75% (t75–t80 after start of baseline recording) that was significantly reduced to only 128.12 ± 3.41% in AAV-Venus-injected cDKO mice (one-way ANOVA followed by Bonferroni's *post hoc* test, $^{\#\#\#}P < 0.001$; Fig 2B). In contrast, the LTP curve recorded from acute slices of AAV-APPsα-injected cDKO mice ($n = 24$) closely overlapped with that of AAV-Venus-injected LM controls (Fig 2A). Quantification of the last 5 min of recording revealed that APPsα rescued LTP deficits of cDKO mice to a level statistically indistinguishable from that of Venus-injected LM controls (t75–80: 150.34 ± 3.55%, $^{ns}P > 0.05$; Fig 2B). While basal synaptic transmission was comparable in all groups (see Fig EV3A and B), presynaptic function evaluated by paired pulse facilitation (PPF; Fig 2C) was significantly impaired in AAV-Venus-injected cDKO mice at the 10 ms ($^{\#}P < 0.05$) and 20 ms ($^{\#}P < 0.05$) interstimulus intervals (ISI) in comparison with AAV-Venus-injected LM controls. Strikingly, AAV-APPsα treatment leads to a highly significant rescue of short-term synaptic plasticity in cDKO mice as evidenced by PPF values statistically indistinguishable from LM controls (Fig 2C).

Next, we evaluated spine density as a correlate of excitatory synapses. To visualize neuronal morphology and spine density, we performed iontophoretic postfixation filling with a fluorescent dye of hippocampal CA1 pyramidal cells in brain slices from injected adult mice (aged 5–6 months). Consistent with our previous study (Hick *et al*, 2015), we confirmed a prominent reduction in spine density both in basal (100.00 ± 3.41 vs. 88.77 ± 3.10 spines/μm, $^{\#}P < 0.05$) and in midapical dendrites (100.00 ± 3.57 vs. 82.08 ± 4.73 spines/μm, $^{\#}P < 0.05$) of AAV-Venus-injected cDKO CA1 neurons as compared to AAV-Venus-injected LM controls (Fig 2D–F). In contrast, spine density of AAV-APPsα-injected cDKO mice did not significantly differ from that of AAV-Venus-injected LM control neurons, indicating that APPsα expression fully restored spine density in CA1 neurons. Collectively, these data demonstrate that acute expression of APPsα in adult mice is sufficient to rescue morphological and functional synaptic deficits in cDKO animals.

APPsα ameliorates dendritic branching abnormalities of cDKO animals

Prompted by the effect of APPsα on spine density, we further evaluated its influence on the overall morphology and complexity of hippocampal CA1 neurons (Fig 3). In view of their different morphology and connectivity, basal and apical dendrites of CA1 neurons were studied separately. Neurons of AAV-Venus-injected cDKO mice showed a significantly reduced total dendritic length and branching (as assessed by the number of nodes) in both basal and apical dendrites compared to AAV-Venus-injected LM controls (Fig 3A–F). Impairments were readily apparent when visually inspecting reconstructed images of individual neurons (Fig 3A).

Although total dendritic length was not significantly increased by APPsα expression in cDKO animals, the total number of nodes was significantly increased in basal dendrites of neurons from AAV-APPsα-injected cDKO mice (Fig 3D) compared to Venus-injected cDKO animals (one-way ANOVA followed by Bonferroni's *post hoc* test, $^{*}P < 0.05$). To investigate whether changes in dendritic complexity may be more pronounced in distinct dendritic subregions, we performed morphometric Sholl analysis. We plotted the dendritic length measured within circles centered on the soma against the distance from the cell body (see scheme in Fig 3B). In this analysis, an increase in dendritic length per sphere corresponds to an increased dendritic complexity. Comparison of dendritic complexity between pyramidal neurons from AAV-Venus-injected cDKO and LM control mice revealed an overall reduced dendritic complexity in cDKO neurons, both in basal (Fig 3G) and apical dendrites (Fig 3H). Branching deficits of basal dendrites from Venus-injected cDKO neurons were most pronounced in proximal dendritic segments (30–90 μm from the soma). In apical dendrites, both proximal regions (60–180 μm) and midapical regions (300 μm, 330 μm) were less complex. Interestingly, neurons of AAV-APPsα-injected cDKO mice exhibited an intermediate curve with partially restored dendritic complexity. Sholl analysis revealed significantly increased dendritic complexity in proximal regions (60 μm) of basal

Figure 3. APPsα ameliorates dendritic branching abnormalities of cDKO animals.

A Representative 3D-reconstructions of CA1 pyramidal neurons from AAV-Venus-injected LM controls (left), AAV-Venus-injected cDKOs (middle, red), and AAV-APPsα-injected cDKOs (right, green).

B Schematic representation of parameters assessed.

C–F Compared to LM controls, AAV-Venus-injected cDKO mice show a significantly reduced basal ($^{\#\#}P < 0.01$, C) and apical ($^{\#\#}P < 0.01$, E) dendritic length and reduced branching in basal ($^{\#\#}P < 0.01$, D) and apical ($^{\#\#}P < 0.01$, F) dendrites. AAV-APPsα injection did neither affect basal ($^{ns}P > 0.05$, C) nor apical ($^{ns}P > 0.05$, E) total dendritic length. However, the total number of basal nodes differed significantly compared to AAV-Venus-injected cDKO mice ($^{*}P < 0.05$, D).

G Sholl analysis of basal dendritic length reveals a significant group effect (repeated measures ANOVA: genotype $F(2, 29) = 5.038$, $P < 0.05$) and a significant distance effect (repeated measures ANOVA: genotype $F(5, 145) = 250.2$, $P < 0.0001$). Due to a significant interaction effect (repeated measures ANOVA: genotype $F(10, 145) = 4.466$, $P < 0.0001$), a *post hoc* Sidak's multiple comparison test was performed to further evaluate effects between groups at distinct distances from soma. Compared to Venus-injected, AAV-APPsα injection of cDKO significantly increased basal dendritic length at 60 μm ($^{*}P < 0.05$).

H Sholl analysis of apical dendritic length reveals an overall significant group effect (repeated measures ANOVA: genotype $F(2, 37) = 4.776$, $P < 0.05$) and a significant distance effect (repeated measures ANOVA: genotype $F(18, 666) = 47.54$, $P < 0.0001$). Due to a significant interaction effect (repeated measures ANOVA: genotype $F(36, 666) = 1.640$, $P < 0.05$), a *post hoc* Sidak's multiple comparison test was performed to further evaluate effects between groups at distinct distances from soma. AAV-APPsα expression increased midapical dendritic length at 300 μm ($^{**}P < 0.01$) and 330 μm ($^{**}P < 0.01$) distance from soma compared to AAV-Venus-injected cDKO mice.

Data information: Age of mice: 5–6 months. n = number of neurons (from 4 to 5 animals per condition). Data represent mean ± SEM. Data were analyzed by one-way ANOVA followed by Bonferroni's *post hoc* test (C–F) or repeated measures ANOVA followed by Bonferroni's or Sidak's *post hoc* test (G–H). # indicates significant differences between LM control and cDKO injected with AVV-Venus, * between cDKO injected with AAV-Venus or APPsα, ● between LM control injected with Venus and cDKO injected with AAV-APPsα. $^{ns}P > 0.05$, $^{*/\#/\bullet}P < 0.05$, $^{**/\#\#/\bullet\bullet}P < 0.01$, $^{\#\#\#}P < 0.001$, $^{\#\#\#\#}P < 0.0001$.

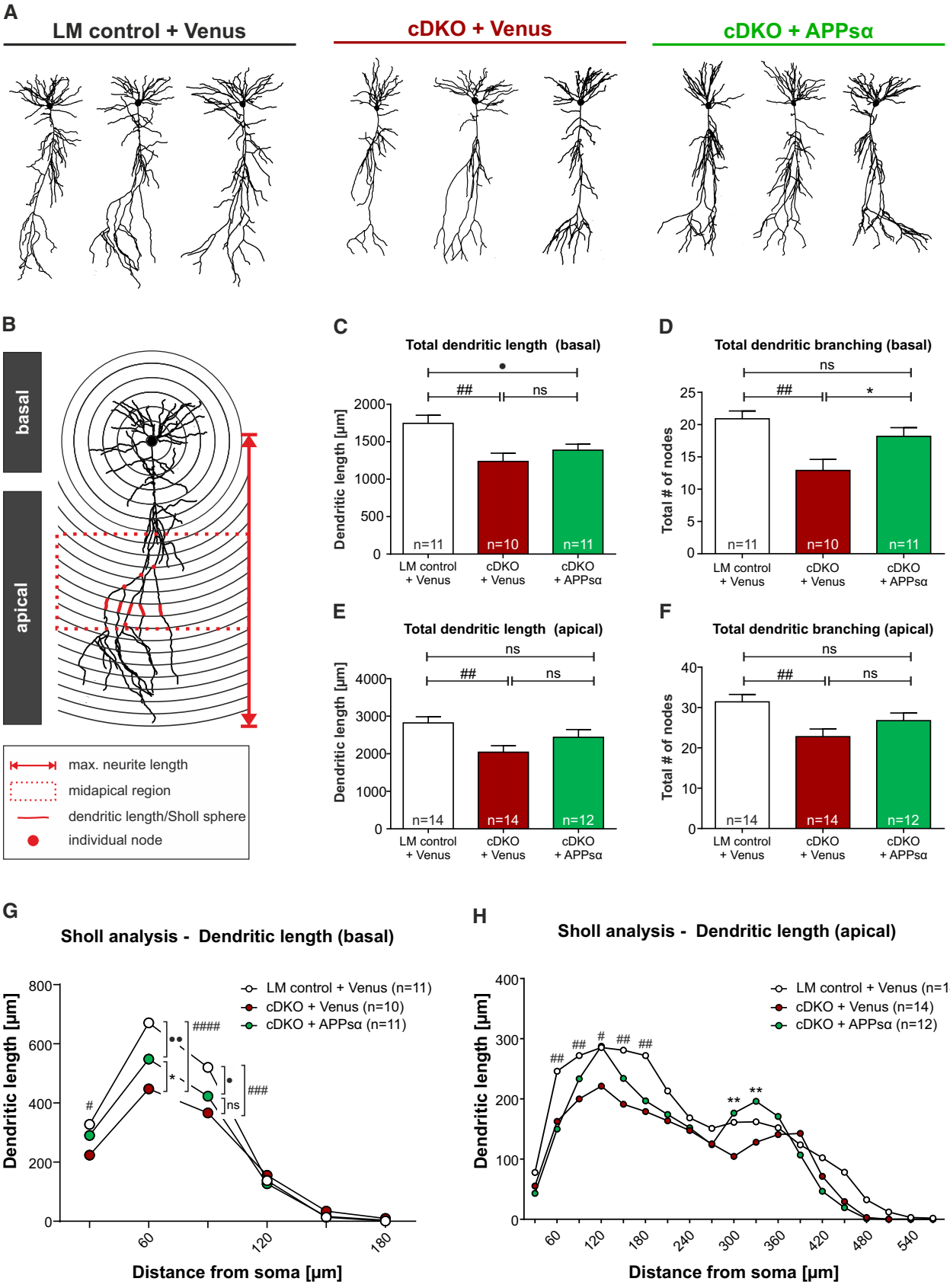

Figure 3.

dendrites of AAV-APPsα-injected cDKO neurons (repeated measures ANOVA followed by Sidak's *post hoc* test, $*P < 0.05$; Fig 3G). Likewise, in apical dendrites of cDKO mice injected with AAV-APPsα, dendritic length was significantly increased at a distance of 300 μm ($**P < 0.01$) and 330 μm ($**P < 0.01$) as compared to neurons of AAV-Venus-injected cDKO neurons. Together, these data indicate that APPsα ameliorates branching deficits of cDKO mice at distinct dendritic regions.

APPsα improves spatial learning and spatial memory in cDKO mice

To evaluate whether improved synaptic density and plasticity is also reflected at the behavioral level, we assessed spatial learning and memory in the Morris water maze (MWM) place navigation task (Fig 4). To this end, cDKO mice were either injected with AAV-Venus ($n = 18$, red circles) or with AAV-APPsα ($n = 18$, green circles) at 4–5 months of age and tested 2 months later at 6–7 months of age. For comparison, LM controls were injected with AAV-Venus ($n = 22$, white circles). While swim speed was comparable in all groups (Fig 4A), we observed an overall impaired performance in AAV-Venus-injected cDKO mice both during acquisition and reversal training. Although all three groups of mice did show learning, escape latencies (Fig 4B) and swim path lengths (Fig 4C) were significantly increased in Venus-injected cDKO mice compared to Venus-injected LM controls, especially at days 2 and 3 of acquisition, learning and for the last trials of reversal learning. These data are highly consistent with and confirm the deficit in spatial learning observed previously in uninjected cDKO mice (Hick *et al*, 2015). Overall, APPsα expression in cDKO mice leads to an intermediate performance with significantly improved learning during the reversal phase. AAV-APPsα expression in cDKO mice significantly decreased escape latency ($**P < 0.01$; Fig 4B) and swim path length ($*P < 0.05$; Fig 4C) at day 5 of reversal learning, as compared to AAV-Venus-injected cDKO mice. During the probe trial that assesses spatial reference memory, analysis of time [%] spend in the target zone (Fig 4D) reveals a significant overall group × place effect ($F(2, 46) = 9.095$, $P = 0.0005$). AAV-Venus-injected cDKO mice were strongly impaired in comparison with AAV-Venus-injected controls ($^{\#\#\#}P < 0.001$) and failed to prefer the trained target zone. Time spend in the target zone was not significantly different from chance level. Strikingly, AAV-APPsα expression substantially improved probe trial performance in cDKO mice compared to Venus-injected cDKO mice ($**P < 0.01$). Moreover, AAV-APPsα-injected cDKOs showed a highly significant preference for the trained target zone over adjacent quadrants ($**P < 0.01$). Together, these data indicate that expression of APPsα in the adult hippocampus substantially improved spatial reference memory.

APPsβ does not rescue LTP or spine density *in vivo*

During AD, BACE expression is upregulated (Holsinger *et al*, 2002; Ahmed *et al*, 2010) leading to increased amyloidogenic APP processing and thus increased APPsβ levels. Although APPsβ has been reported to be less potent in assays of neuroprotection *in vitro* (Furukawa *et al*, 1996; Barger & Harmon, 1997; Copanaki *et al*, 2010), the molecular basis of this property has remained elusive and its *in vivo* role is currently unknown. We therefore evaluated in a separate set of experiments whether APPsβ, being only 16 amino acids shorter compared to APPsα (see Fig 5B), might also be able to rescue the impairments of cDKO mice. Briefly, we stereotactically injected cDKO mice and LM controls (4–5 months of age) with AAV-Venus or a bicistronic vector coding for Venus and HA-tagged murine APPsβ (AAV-APPsβ; Fig 5A). Immunohistochemistry of serial brain sections indicated that injection of AAV-APPsβ yielded a comparable expression level and distribution to that obtained for HA-APPsα (Figs 5C and EV1C). Western blot analysis of total hippocampal homogenates (containing cell bound and secreted proteins) using an HA-tag-specific antibody further confirmed similar (and statistically not significantly different) levels of HA-APPsß and HA-APPsα expression upon injection of the respective AAVs (unpaired two-tailed Student's *t*-test, $^{ns}P > 0.05$; Fig 5D and E). Ultracentrifugation (UC) of the same hippocampal homogenates was used to specifically detect soluble HA-APPsα and HA-APPsβ (Fig 5D, lower boxed panels) and yielded comparable levels of APPsα and APPsβ in UC supernatants (unpaired two-tailed Student's *t*-test, $^{ns}P > 0.05$; Fig 5D and E). Transfection of HEK cells (Fig EV2A) with the APPsα or APPsβ encoding AAV plasmids or transduction of cultured neurons with either of the AAV vectors (Fig EV2B) further confirmed efficient and comparable secretion of APPsα or APPsβ, as evidenced by Western blot analysis of cell supernatants (Fig EV2A and B).

Strikingly, despite comparable levels of expression and secretion, soluble APPsβ failed to exert any detectable effects on basal synaptic transmission (Fig EV3C and D) or synaptic plasticity in recordings of cDKO slices at 5–6 months of age (Fig 5F–H). AAV-APPsβ-injected cDKO mice showed superimposable LTP curves compared to Venus-injected cDKO mice. Potentiation at t75–80 min after start of baseline recording was not significantly different (cDKO + AAV-Venus: 125.58 ± 2.69% vs. cDKO + AAV-APPsβ: 124.42 ± 1.96%, $^{ns}P > 0.05$, unpaired two-tailed Student's *t*-test). Moreover, also in the PPF paradigm AAV-APPsβ expression did not lead to any detectable difference compared to AAV-Venus control injections (Fig 5H). Likewise, and consistent with electrophysiological analysis, AAV-APPsβ failed to rescue spine density deficits of cDKO mice determined upon Golgi staining. AAV-Venus-injected cDKO mice revealed again a significant reduction in spine density in basal and in apical dendrites as compared to Venus-injected LM controls (Fig 5I–K). However, spine density was comparable and statistically indistinguishable in AAV-Venus and APPsβ-injected cDKO mice. Basal dendrites from AAV-Venus and AAV-APPsβ-injected cDKO mice showed a similar and statistically not significantly different reduction in spine density of 14% (LM control + Venus: 100 ± 2.84 vs. cDKO + Venus: 85.99 ± 3.51 spines/μm, $*P < 0.05$) and 12% (LM control + Venus: 100 ± 2.84 vs. cDKO + APPsβ: 88.39 ± 3.26 spines/μm, $****P < 0.0001$), respectively (Fig 5J). In midapical dendritic segments, spine density was reduced by 24% in AAV-Venus-injected cDKO animals (LM control + Venus: 100 ± 4.01 vs. cDKO + Venus: 76.05 ± 2.097 spines/μm) or by 18% (LM control + Venus: 100 ± 4.01 vs. cDKO + APPsβ: 82.40 ± 3.28 spines/μm) in AAV-APPsβ-injected animals, respectively (Fig 5K). Together, these data indicate a striking difference in the *in vivo* properties of secreted APPs, with APPsα ameliorating morphological and functional synaptic deficits of cDKO mice, while APPsβ had no effect.

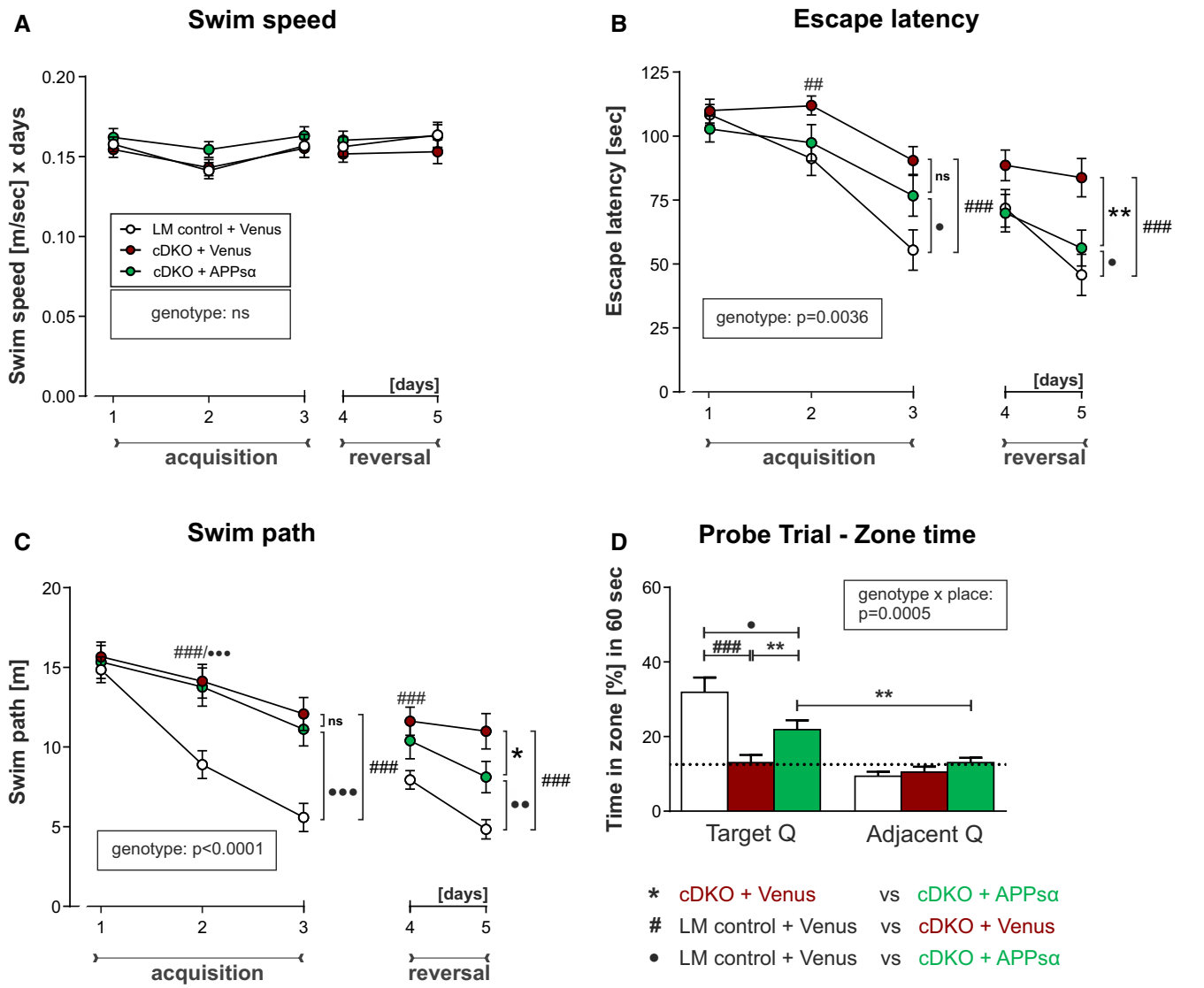

Figure 4. APPsα improves place navigation and spatial memory of cDKO mice in the MWM.

A Swim speed during acquisition and reversal learning is comparable in all groups (each point represents 1 day with six trials).

B During acquisition learning and after platform reversal to the opposite quadrant, AAV-Venus-injected cDKOs (red circles) show considerably longer escape latency compared to AAV-Venus-injected LM controls (white circles). AAV-APPsα-injected cDKO mice (green circles) show an overall intermediate performance (genotype $F(2, 46) = 6.361$, $P = 0.0036$) and that differs significantly at day 5 of reversal learning compared to AAV-Venus-injected cDKO mice (genotype × day $F(8, 184) = 5.266$, $P < 0.0001$; $^{**}P < 0.01$).

C Measurements of swim path length confirm the training performance deficit of cDKO mice compared to LM controls. During the reversal phase, the performance of AAV-APPsα-injected cDKOs is significantly improved at day 5 (genotype $F(2, 46) = 16.70$, $P < 0.0001$, genotype × day $F(8, 184) = 5.788$, $P < 0.0001$; $^{*}P < 0.05$, $^{\bullet\bullet}P < 0.01$).

D In the probe trial, AAV-Venus-injected cDKOs (red) spend significantly less time in the target zone compared to AAV-Venus- ($^{\#\#\#}P < 0.001$) injected LM control animals (white) and failed to prefer it significantly over control zones in adjacent quadrants. Note that expression of APPsα (green) largely rescues the deficits of cDKOs. $N = 22$ (LM controls: AAV-Venus), $N = 18$ (cDKOs: AAV-Venus), $N = 18$ (cDKOs: AAV-APPsα).

Data information: Data represent mean ± SEM. Dashed lines: chance level. Data were analyzed using a mixed ANOVA model with conditions (LM control: AAV-Venus, cDKO: AAV-Venus and cDKO: AAV-APPsα) as between subject factor. Within subject, factors were added to explore the dependence of genotype effects on day and place. Significant interactions and main effects were further explored by pairwise FDR-corrected two-tailed Student's *t*-tests. # indicates significant differences between LM control and cDKO injected with AVV-Venus, * between cDKO injected with AAV-Venus or APPsα, • between LM control injected with Venus and cDKO injected with AAV-APPsα $^{ns}P > 0.05$, $^{*/\bullet}P < 0.05$, $^{**/\#\#/\bullet\bullet}P < 0.01$, $^{\#\#\#/\bullet\bullet\bullet}P < 0.001$.

APPsα facilitates LTP via its C-terminal CTα16 domain

Prompted by these results, we now focused on the 16 amino acids domain (CTα16) that distinguishes APPsα from APPsβ (Fig 5B and L–Q). Previously, we had demonstrated that a short incubation of slices with recombinant APPsα (recAPPsα) is sufficient to largely rescue the LTP deficits of cDKO mice (Hick *et al*, 2015). To determine whether this acute function of APPsα is mediated by the

CTα16 domain, we now pre-incubated cDKO slices for 60 min at room temperature either with a synthetic CTα16 peptide (10 nM), or with $CT\alpha16_{scr}$ (10 nM), a scrambled peptide of the same amino acid composition. After 20 min of baseline recording, LTP was again induced by TBS. During the whole measurement, the peptides diluted in ACSF were circulating in a closed-loop system. Strikingly, we found that the application of CTα16 potently facilitated LTP over the whole recording period (Fig 5L and M) including the early phase of post-tetanic potentiation (t20–25, CTα16: 191.49 ± 8.82% vs. $CT\alpha16_{scr}$: 165.12 ± 8.82%, $^{*}P < 0.01$; Fig 5L and M) and led to a highly significant increase in LTP values 60 min after TBS (t75–80, CTα16: 148.08 ± 3.65% vs. $CT\alpha16_{scr}$: 132.18 ± 4.26%, $^{**}P < 0.01$; Fig 5L and M). In contrast, LTP values obtained for $CT\alpha16_{scr}$ were very similar to those after AAV-Venus-injection into cDKO mice (t75–80, 128.12 ± 3.41%; Fig 2B). CTα16 peptide application also significantly improved and restored PPF of cDKO slices (Fig 5N) to values comparable to that obtained for AAV-Venus-injected LM control mice (see Fig 2C). Next, we directly compared the activity of CTα16 and recAPPsα (Fig 5O–Q) that was purified from stably transfected HEK cell supernatants. We found that CTα16 application (10 nM) was as potent as recAPPsα (10 nM) in rescuing both the LTP (t75–80, APPsα: 146.15 ± 4.21% vs. CTα16: 148.08 ± 3.65%, $^{ns}P > 0.05$) and PPF deficit of cDKO slices. Values obtained were statistically indistinguishable (Fig 5O and P). Together, these data identify the CTα16 domain of APPsα as sufficient to mediate the functions of APPsα for enhancing synaptic plasticity *in vitro*.

Inhibition of α7-nAChR by BTX blocks APPsα-mediated effects on LTP

While elevated (micromolar) Aβ concentrations and aggregated Aβ species exert an inhibitory effect on synaptic function (Kamenetz *et al*, 2003; Shankar *et al*, 2007; Gu & Yakel, 2011), picomolar concentrations of soluble Aβ have previously been demonstrated to enhance LTP and PTP in a mechanism dependent on the activity of α7 nicotinic acetylcholine receptors (α7-nAChRs; Puzzo *et al*, 2011, 2008). As the CTα16 domain of APPsα overlaps with the N-terminus of Aβ, we therefore tested whether signaling by α7-nAChR may mediate the LTP facilitating functions of APPsα. First, we hypothesized that if α7-nAChRs are crucially involved in the LTP facilitating effect of APPsα, pharmacological block of α7-nAChR should impair LTP in LM control mice that still express APP and APPsα. Indeed, treatment of slices with 10 nM α-bungarotoxin (α-BTX), a specific inhibitor of α7-nAChRs, significantly reduced LTP during the induction phase (t20–25, LM control: 184.01 ± 5.59% vs. LM control + BTX: 158.04 ± 8.35%, $^{*}P < 0.05$) and the maintenance phase (t75–80, LM control: 147.25 ± 3.87% vs. LM control + BTX: 131.24 ± 4.99%, $^{*}P < 0.05$; Fig 6A and B). Values obtained after BTX treatment were very similar to those of $CT\alpha16_{scr}$-treated cDKO

Figure 5. AAV-APPsβ fails to rescue LTP or spine density *in vivo*, while CTα16 facilitates LTP *in vitro*.

A Schematic representation of AAV9 constructs enabling the neuron-specific expression of (i) Venus and (ii) HA-tagged APPsβ (+Venus). ITR: inverted terminal repeat, Synapsin: neuron-specific promotor, T2A: *Thoseaasigna* virus 2A site, SP: signal peptide, HA: influenza hemagglutinin tag.

B APPsα differs from APPsβ in the last 16 C-terminal amino acids (CTα16, green). The epitope recognized by the M3.2 antibody is indicated.

C Overview of the hippocampus of a AAV-APPsβ- (HA-tag, red) injected cDKO mouse. APPsβ is expressed in CA1, CA3, and DG. Scale bar: 500 μm. DG: dentate gyrus, CA: Cornu Ammonis.

D Western blot analysis of HA-APPsα and HA-APPsβ in hippocampi of injected mice (boxed upper panel) probed with an HA-tag-specific antibody (lower band, arrowhead; *unspecific signal). Homogenates of AAV-injected hippocampi were subjected to ultracentrifugation to detect soluble APPsα and APPsβ (UC supernatant; boxed lower panel). The APP C-terminal antibody Y188 was used to confirm the separation of soluble APPsα from membrane bound full-length APP that is detected in total lysates of AAV-Venus-injected littermate controls. Hippocampi of $APP^{-/-}$ mice served as a negative control for antibody specificity.

E Quantification of HA-APPsα and HA-APPsβ expression in total hippocampal homogenates and of soluble HA-APPs after UC normalized to β-tubulin. Note the comparable expression in AAV-APPsα- and AAV-APPsβ-injected mice. Age: 5–6 months. *N* = Number of animals. Data represent mean ± SEM. Data were analyzed by unpaired two-tailed Student's *t*-test. $^{ns}P > 0.05$.

F–H Activity-dependent synaptic plasticity was investigated in cDKO after injection of AAV-Venus (red) or APPsβ (blue). (F, G) AAV-mediated overexpression of APPsβ (*n* = 23 slices, blue symbols) failed to rescue the LTP defect of cDKO mice (*n* = 24 slices, red symbols). (G) TBS-induced strengthening of fEPSPs resulted in similar potentiation levels for the last 5 min of recording (t75–80). The LTP induction rate is shown as percentage % of mean baseline slope. Data points were averaged over six time points. (H) PPF paradigm yielded no significant differences between viral vector-injected cDKO mice. Age: 5–6 months. *n* = number of recorded slices. *N* = number of animals. Data represent mean ± SEM. Data were analyzed by unpaired two-tailed Student's *t*-test.

I Representative images of Golgi-stained midapical and basal dendritic segments of LM control and cDKO animals injected with AAV-Venus or AAV-APPsβ. Images are maximum projections of *z*-stacks. Scale bar: 5 μm.

J, K The significant spine density deficit of AAV-Venus-injected cDKO mice (red bar) in basal (J) and apical dendrites (K) was comparable and not significantly different ($^{ns}P > 0.05$) from that of AAV-APPsβ-injected cDKO mice (blue bar). White bar: AAV-Venus-injected LM controls. Spine density is normalized to LM control levels. Age: 5–6 months; *n* = number of neurons (from five animals per condition). Data represent mean ± SEM. Data were analyzed by one-way ANOVA followed by Bonferroni's *post hoc* test. $^{*}P < 0.05$, $^{**}P < 0.01$, $^{****}P < 0.0001$.

L, M Acute hippocampal slices of cDKO were pre-incubated for 1 h either with 10 nM CTα16 or $CT\alpha16_{scr}$ before inducing LTP by TBS (arrowhead). Averaged potentiation levels at LTP induction (t20–25) revealed a significantly enhancement by CTα16 as compared to $CT\alpha16_{scr}$ present over the whole recording time. Potentiation levels at t75–80 are significantly increased in the presence of CTα16 ($^{**}P < 0.01$). The LTP induction rate is shown as percentage % of mean baseline slope. Data points were averaged over six time points. $^{*}P < 0.05$, $^{**}P < 0.01$. *n* = number of recorded slices. *N* = number of animals. Data represent mean ± SEM. Data were analyzed by unpaired two-tailed Student's *t*-test.

N CTα16 significantly enhances short-term synaptic plasticity at inter-stimulus intervals of 40 ($^{**}P < 0.01$), 80 ($^{*}P < 0.05$), and 160 ($^{**}P < 0.01$) ms compared to $CT\alpha16_{scr}$. *n* = number of recorded slices. *N* = number of animals. Data represent mean ± SEM. Data were analyzed by unpaired two-tailed Student's *t*-test.

O–Q Acute application of CTα16 and recAPPsα elevates LTP in cDKO slices to the same extent. (O, P) After 1 h pre-incubation with either 10 nM CTα16 or 10 nM recAPPsα, fEPSPs were recorded. The TBS-induced LTP curve was closely overlapping for both conditions and resulted in similar, statistically not significantly different LTP values. (Q) CTα16 and recAPPsα modulate presynaptic function of cDKO mice in the same manner. Age: 5–6 months. *n* = number of recorded slices. *N* = number of animals. Data represent mean ± SEM. Data were analyzed by unpaired two-tailed Student's *t*-test.

Source data are available online for this figure.

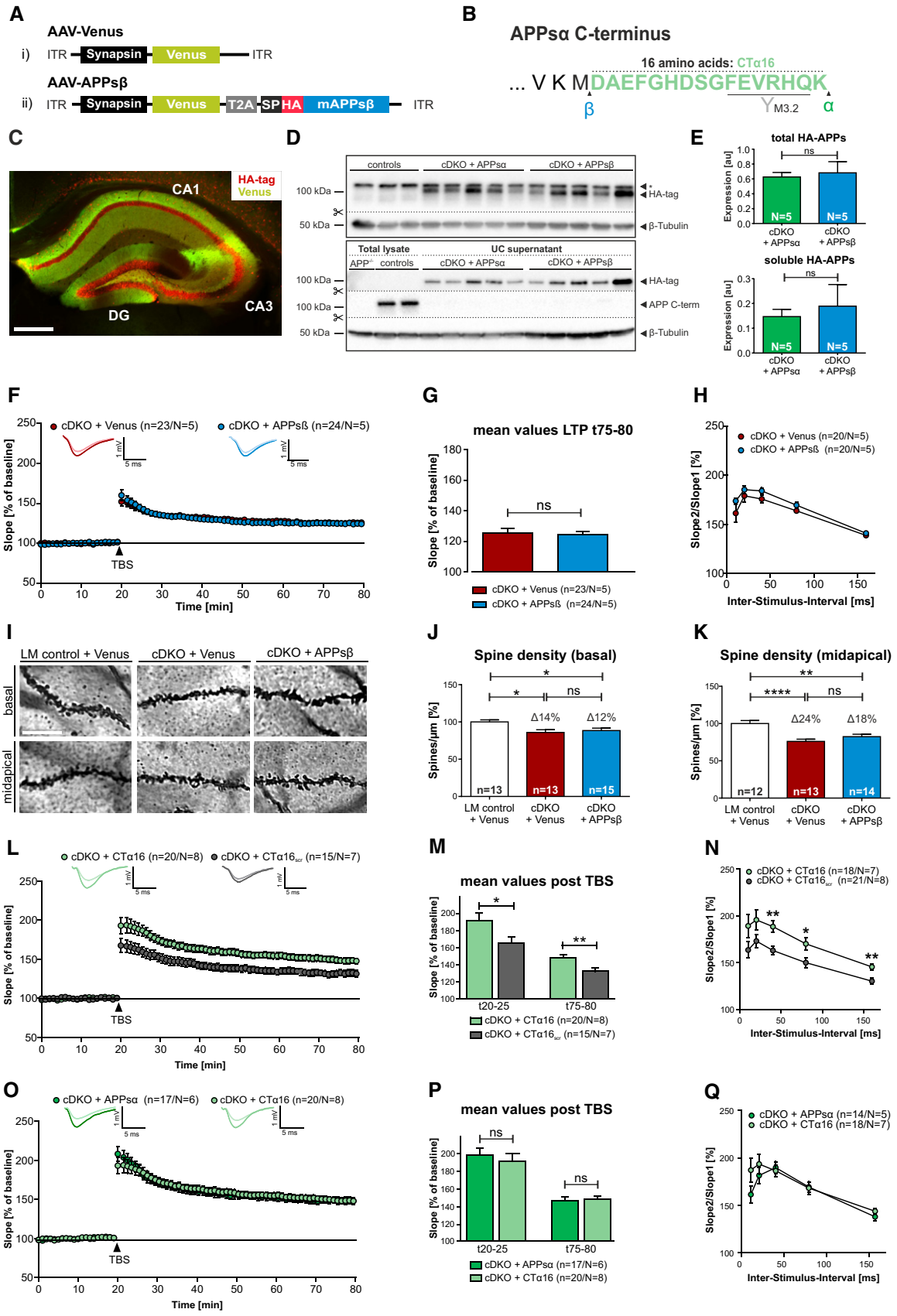

Figure 5.

slices (compare to Fig 5L and M, CTα16$_{scr}$-treated cDKO slices: 132.18 ± 4.26%).

Next, we tested how α-BTX affects the induction of LTP by exogenous application of recAPPsα or CTα16 (Figs 6C–G and EV4). When α-BTX was added after the incubation of slices with either recAPPsα or CTα16 30 min before TBS (Fig EV4A, scheme), we observed only a small but not significant reduction in LTP (Fig EV4B–E). In contrast, if α-BTX was co-applied together with recAPPsα for 1 h before TBS (Fig 6C, scheme), this leads to a significant inhibition as compared to recAPPsα treatment alone (Fig 6D and E) both during the LTP induction phase (t20–25, recAPPsα: 168.49 ± 7.20% vs. recAPPsα + BTX: 142.57 ± 7.75%, $^{*}P < 0.05$; Fig 6D and E) and the LTP maintenance phase (t75–80, recAPPsα: 135.59 ± 3.81% vs. recAPPsα: +BTX: 118.58 ± 5.51%, $^{*}P < 0.05$; Fig 6D and E). Similarly, if α-BTX was co-applied together with the CTα16 peptide for 1 h before TBS (Fig 6F and G), this lead to a significant inhibition as compared to CTα16 treatment alone both during the LTP induction phase (t20–25, CTα16: 176.23 ± 4.69% vs. CTα16 + BTX: 153.75 ± 5.05%, $^{*}P < 0.05$; Fig 6F and G) and the LTP maintenance phase (t75–80, CTα16: 144.37 ± 2.34% vs. CTα16 + BTX: 129.24 ± 3.40%, $^{**}P < 0.01$; Fig 6F and G). Together, these data suggest that APPsα exerts its functions on LTP mainly via the CTα16 domain in a mechanism depending on α7-nAChR function. Further studies are needed to address whether improvements in spine density and behavior that we observed upon AAV-APPsα re-expression might also depend on α7-nAChR function.

APPsα shows high-affinity allosteric potentiation of α7-nAChR expressed in *Xenopus* oocytes

To investigate whether CTα16 can modulate α7-nAChRs directly, homomeric α7-nAChRs were expressed in *Xenopus laevis* oocytes, and nicotine- or acetylcholine-induced currents at submaximal EC_{50} agonist concentration (100 μM) were measured either alone or after pre-application of CTα16 by two-electrode voltage clamp. Upon application of 100 nM of CTα16 alone, no activation of α7-nAChRs was detectable (data not shown). Remarkably, 100 nM of CTα16 significantly potentiated both nicotine- and acetylcholine-induced currents with a 2.58 ± 0.42-fold ($n = 8$) and 3.01 ± 0.96-fold ($n = 7$) enhancement of α7-nAChRs responses, respectively (paired two-tailed Student's *t*-test, $^{*}P < 0.05$; Fig 7A and B). In contrast, no significant effect of 100 nM CTα16$_{scr}$ on nicotine-induced currents could be detected (1.00 ± 0.06-fold increase, paired two-tailed Student's *t*-test, $n = 5$; $^{ns}P > 0.05$; Fig 7A and B). Dose-response analysis of CTα16 concentrations between 1 and 100 nM yielded an EC_{50} value for CTα16 of 10.7 ± 4.6 nM with an hill coefficient of 2.1 ± 0.3 for α7-nAChRs ($n = 4$; Fig 7C). To establish whether the physiological APPsα fragment that contains the CTα16 sequence at the C-terminus can also modulate α7-nAChRs, we tested the effect of 20 nM recAPPsα, a concentration close to the 10 nM that facilitated LTP in slices, on nicotine-gated currents (Fig 7D–F). Indeed, 20 nM recAPPsα significantly potentiated nicotine-induced currents (3.35 ± 0.81-fold enhancement, paired two-tailed Student's *t*-test, $n = 4$; $^{*}P < 0.05$) to a similar extent as seen with 100 nM of CTα16 (Fig 7D and E, see Fig 7A for comparison). This effect could be specifically blocked by BTX (Fig 7D). Notably, and consistent with experiments in slices, no significant potentiation was seen upon pre-application of 20 nM recAPPsβ (1.32 ± 0.18-fold enhancement, paired two-tailed Student's *t*-test, $n = 5$, $^{ns}P > 0.05$; Fig 7D and E). As a further control, we investigated whether APPsα may also modulate other pentameric ion channels. However, neither recAPPsα nor CTα16 had any effects on the structurally related homomeric α1-GlyR (Fig EV5), indicating that APPsα specifically acts on α7-nAChRs. Next, to gain further mechanistic insight, we analyzed nicotine dose-responses of α7-nAChRs in the presence of a potentiating concentration of recAPPsα to see how APPsα modulates α7-nAChRs (Fig 7F). Strikingly, 20 nM recAPPsα shifted the nicotine dose–response curve to the left and lead to an approximately twofold significant decrease in the EC_{50} of nicotine (40.3 ± 6.0 μM) as compared to recAPPsα-free conditions (EC_{50} of 80.5 ± 12.7 μM, paired two-tailed Student's *t*-test, $n = 5$, $^{*}P < 0.05$) without affecting the hill coefficient (3.3 ± 0.5 vs. 3.7 ± 0.9, paired two-tailed Student's *t*-test, $^{ns}P > 0.05$) and the maximal inducible nicotine currents (Fig 7F). Together, these data indicate that APPsα acts as a potent (nanomolar range) positive allosteric modulator of α7-nAChRs by increasing the apparent agonist affinity.

Discussion

In this study, we provide compelling evidence for distinct functional roles of the two secreted APP ectodomain fragments APPsα and APPsβ *in vivo* and provide functional insight into the underlying

Figure 6. LTP facilitation by APPsα or CTα16 requires functional α7-nAChRs.

A, B Treatment with 10 nM α-BTX (30 min prior to TBS, black circles) significantly reduces LTP induction (t20–25, phase of post-tetanic potentiation) and maintenance (t75–80) in LM controls expressing endogenous APP and APPsα. The LTP induction rate is shown as percentage % of mean baseline slope. Data points were averaged over six time points.

C Experimental setup: co-application of recAPPsα or CTα16 and BTX before LTP induction. Peptides and BTX inhibitor used for pre-incubation circulated throughout the whole LTP recording.

D, E Co-application of BTX and recAPPsα significantly inhibits synaptic plasticity in cDKO mice. After 1 h pre-incubation of acute slices with 10 nM recAPPsα or 10 nM recAPPsα and 10 nM BTX, fEPSPs were recorded. Hippocampal acute slices treated with 10 nM BTX and recAPPsα revealed significantly impaired induction (t20–25) and maintenance (t75–80) of LTP in comparison with slices of cDKO mice recorded in the presence of recAPPsα alone.

F, G Co-application of BTX and CTα16, the C-terminal domain of APPsα, significantly inhibits synaptic plasticity in cDKO mice. After 1 h pre-incubation of acute slices with 10 nM CTα16, or 10 nM CTα16 and 10 nM BTX, fEPSPs were recorded. Hippocampal acute slices treated with 10 nM BTX and CTα16 revealed similar to recAPPsα, a significantly impaired induction (t20–25) and maintenance (t75–80) of LTP in comparison with slices of cDKO mice recorded in the presence of CTα16 alone.

Data information: Age: 5–6 months of age. *n* = number of recorded slices. *N* = number of animals. Data represent mean ± SEM. Data were analyzed by unpaired two-tailed Student's *t*-test. $^{*}P < 0.05$, $^{**}P < 0.01$.

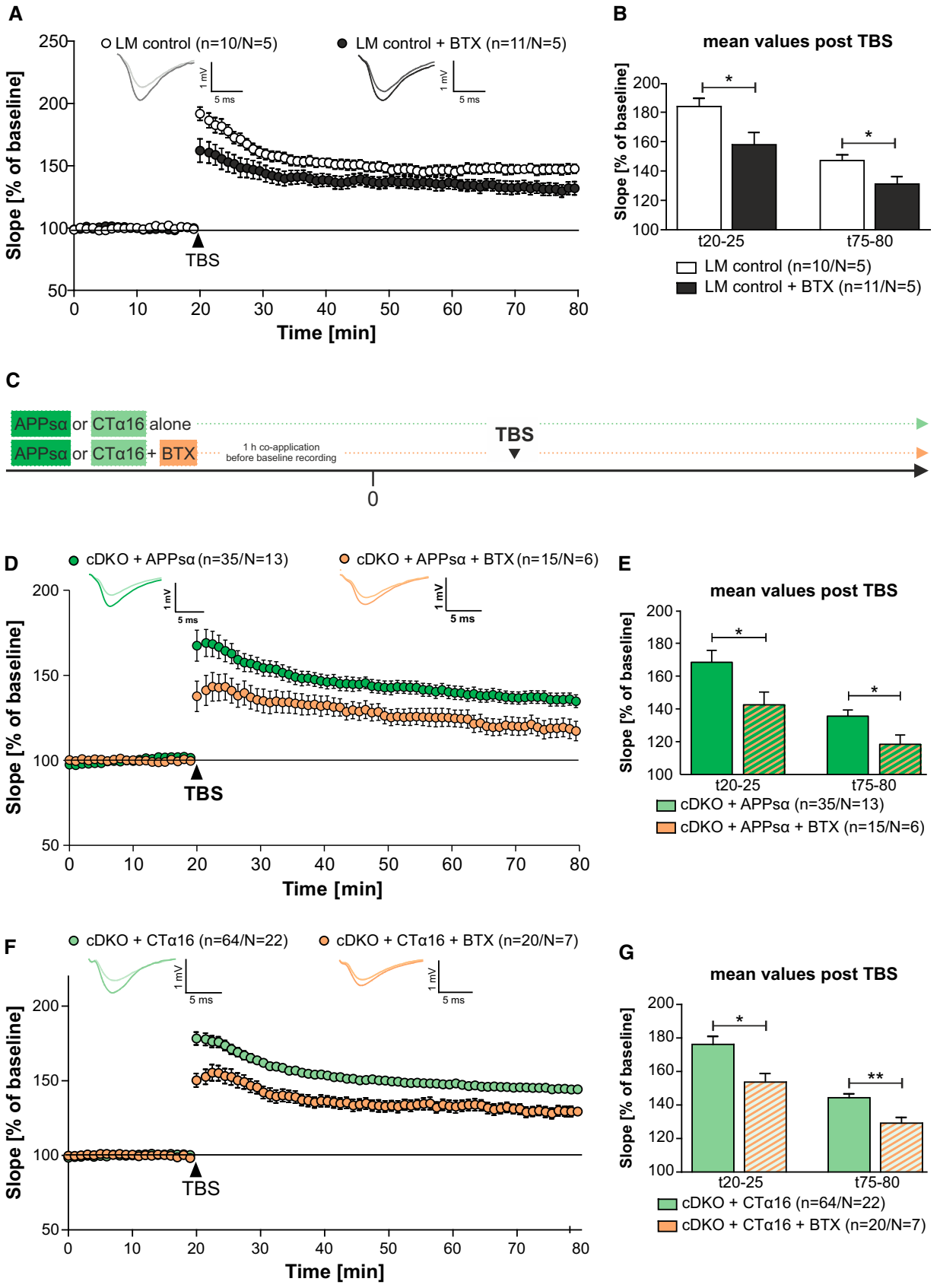

Figure 6.

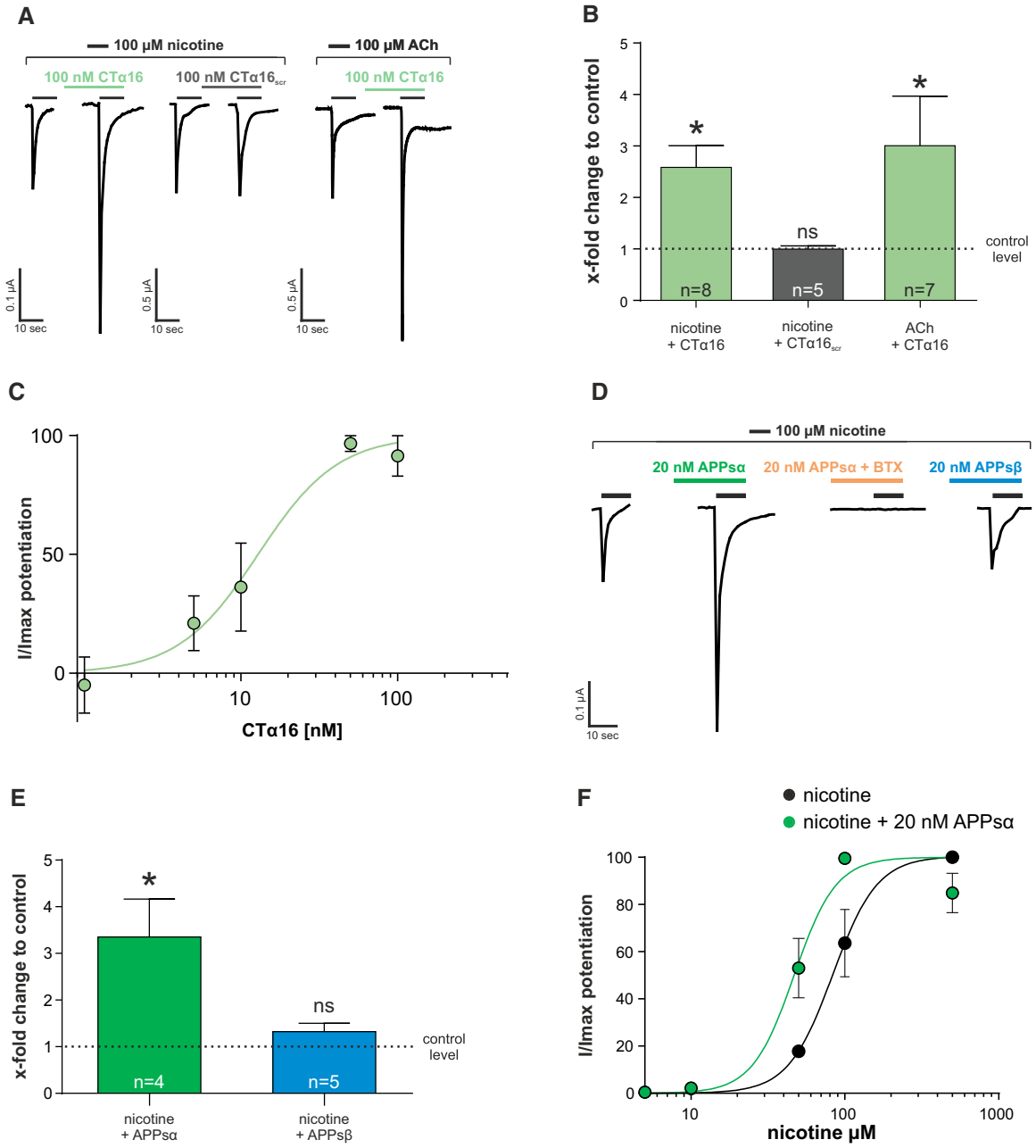

Figure 7. Potentiating effect of CTα16 and APPsα on recombinant homomeric α7-nAChRs.

A Nicotine- and acetylcholine-induced whole-cell current traces of α7-nAChRs expressed in *Xenopus* oocytes recorded in the absence or presence of CTα16 or $CTα16_{scr}$, respectively. Note specific robust potentiation of nicotine- and acetylcholine-induced currents by CTα16, but no direct activation of α7-nAChRs by either peptide in the absence of agonist (not shown). Bars indicate application of EC_{50} agonist concentrations and of the peptide indicated (green: CTα16: gray: $CTα16_{scr}$).

B Quantification of potentiation shows that CTα16 enhances nicotine- and acetylcholine-induced currents to a similar extend, whereas $CTα16_{scr}$ had no effect.

C CTα16 dose–response curve obtained with submaximal nicotine concentrations (100 µM) with a corresponding EC_{50} value of 10.7 ± 4.6 nM and a hill coefficient of 2.1 ± 0.3 (n = 4).

D Nicotine-induced whole-cell current traces of α7-nAChRs in the presence of 20 nM recAPPsα (green bar) or 20 nM recAPPsβ (blue bar). Note that only recAPPsα efficiently potentiates α7-nAChRs, which is blocked by BTX (orange bar).

E Quantification of potentiation shows that recAPPsα enhances nicotine-induced currents to a similar extend as CTα16 (see for comparison Fig 7B) while recAPPsβ had no effect.

F Nicotine dose–response curve obtained either in the presence of 20 nM recAPPsα (green circles, left) or without treatment (black circles, right). Note that recAPPsα treatment shifts the curve to the left, significantly reducing the apparent agonist affinity by about twofold (EC_{50} of 40.3 ± 6.0 µM, green curve vs. EC_{50} of 80.5 ± 12.7 µM, black curve; n = 5).

Data information: For statistical evaluation of potentiation, we performed a paired two-tailed Student's t-test of the agonist-induced currents in the absence and presence of the indicated peptide. n = number of oocytes. Data represent mean ± SEM. $^{ns}P > 0.05$, $^{*}P < 0.05$.

mechanism. Long-term AAV-mediated expression of either APPsα or APPsβ in the hippocampus of adult NexCre cDKO (cDKO) mice revealed several important new findings: (i) *In vivo* expression of APPsα efficiently rescued deficits in spine density, synaptic plasticity (LTP and PPF) and spatial reference memory of cDKO mice. (ii) In contrast to APPsα, APPsβ expression had no detectable effects on spine density and synaptic plasticity in cDKO mice indicating distinct functional roles in the adult CNS. (iii) The C-terminal 16 amino acids (CTα16) of APPsα proved sufficient to enhance LTP to the same extent as full-length APPsα. (iv) Nanomolar concentrations of APPsα and CTα16 function as potent positive allosteric modulators of α7-nAChRs *in vitro* increasing the apparent agonist affinity. (v) Pharmacological blockade of α7-nAChRs impaired the APPsα (or CTα16)-induced LTP facilitation, thus identifying α7-nAChRs as physiological APPsα receptors that are involved to mediate its LTP-enhancing effects.

Our previous studies indicated that LTP deficits of cDKO mice can be rescued by acute application of nanomolar amounts of APPsα, but not APPsβ, *in vitro*. Despite this, it remained unclear whether these acute *in vitro* effects observed for a short time of recording would also be relevant *in vivo* and whether reduced spine density and behavioral deficits might also be rescued. Lastly, the mechanism by which APPsα regulates LTP including the relevant receptor was unknown. In principle, synaptic deficits of cDKO mice may either arise from developmental deficits such as impaired synaptogenesis that could lead to miswired circuits or may be due to a lack of APP (or APLP2)-mediated functions in the adult brain. To address these questions and to assess the specific role(s) of the secreted ectodomains APPsα and APPsβ, we used a reverse genetic approach employing AAV-mediated re-expression of APPsα or APPsβ in the hippocampus of adult cDKO mice. Expression of the AAV-Venus control vector in cDKO mice or littermate controls fully reproduced and confirmed the phenotype of cDKO mice (Hick *et al*, 2015) including reduced dendritic complexity (Fig 3) and spine density of CA1 neurons (Fig 2), deficits in synaptic plasticity (Fig 2), and impaired spatial memory (Fig 4). This indicates that the cDKO phenotype is robust and that AAV vectors are suitable to confer neuron-specific, long-lasting and widespread expression throughout the dorsal hippocampus (see Figs 1 and EV1). Using this *in vivo* reconstitution approach, we show that APPsα is not only able to acutely modulate synaptic strength when applied *in vitro* (Hick *et al*, 2015), but has the ability to mediate a long-lasting rescue of synaptic plasticity, with facilitating effects on both the induction and maintenance phase of LTP. Moreover, we show that APPsα re-expression rescued spine density, a correlate of excitatory synapses. These data are perfectly in line with our recent observation that a lack of APP and thus APPsα in APP-KO mice leads to impairments in structural spine plasticity in the cortex (Zou *et al*, 2016). While synaptic plasticity and spine density were completely restored, APPsα expression led only to a partial rescue of dendritic complexity of CA1 neurons with effects most pronounced close to the soma and in the midapical region of apical dendrites. These more subtle effects might in part be related to a potential non-uniform secretion of APPsα along dendritic regions of individual neurons that may become limiting at more distant regions. Alternatively, it is conceivable that APPsα is not sufficient to fully restore neurite outgrowth and dendritic arbors due to an inability to compensate early developmental defects or an additional requirement for APLP2 (Weyer *et al*, 2014; Hick *et al*, 2015). In this regard, neither deficiency of APP nor APLP2 alone results in reduced dendritic complexity in young adult knockout mice (Lee *et al*, 2010; Midthune *et al*, 2012; Tyan *et al*, 2012), while a combined absence in cDKO mice profoundly impairs neuronal morphology and total neurite length (Hick *et al*, 2015; Weyer *et al*, 2014 and this study) indicating a combined role of APP and APLP2 for dendritic complexity. Although the underlying mechanism is still unknown, it appears likely that domains conserved between APP and APLP2 (and not divergent sequences as those close to the secretase sites) are involved.

The ability of synapses to undergo long-term potentiation is considered as a cellular mechanism underlying learning and memory (reviewed by Korte & Schmitz, 2016). Indeed, restoration of LTP by APPsα at the CA3/CA1 pathway was associated with a significantly improved performance in water maze place navigation during reversal learning (Fig 4B and C) and a substantial increase of spatial reference memory, as assessed during the probe trial. In mice, emotional reactions to the swim stress are a limiting factor for performance during task acquisition that becomes less relevant during reversal learning as mice get habituated to the stressful experience (Lipp & Wolfer, 1998; Strange *et al*, 2014). The dorsal hippocampus that is known to mediate spatial processing (Strange *et al*, 2014) was efficiently targeted by AAV-APPsα injections, whereas AAV-APPsα was undetectable in ventral portions of the hippocampus (Fig EV1C) that mediate emotional responses. Thus, a failure to compensate emotional problems due to selective targeting may explain why AAV-APPsα treatment effects were only seen during probe trial and reversal learning. Although hippocampal lesions have been demonstrated to impair hippocampus-dependent behavior (Morris *et al*, 1982), learning and memory also involves other brain regions that were not targeted by the injections including the dorsomedial striatum-prefrontal cortex network which is strongly involved in the initial acquisition of the place navigation task (Woolley *et al*, 2013). The entorhinal cortex constitutes a crucial interface between the hippocampus and the rest of the cortex and is the source of most spatial information that is processed in the hippocampus (Hales *et al*, 2014; Vorhees & Williams, 2014). The fact that AAV-APPsα expression was largely restricted to the hippocampus may thus underlie the partial but not complete rescue of performance by APPsα in the MWM. In addition, part of the behavioral deficits may also be due to developmental effects of the mutation.

Consistent with an important function of APPsα in the mature brain, acute depletion of APPsα in wild-type animals by either pharmacological inhibition of α-secretase (Taylor *et al*, 2008), or infusion of antibodies directed against the C-terminus of APPsα (Taylor *et al*, 2008; Puzzo *et al*, 2011) was reported to impair LTP and cognitive behavior. However, these previous approaches lacked specificity, as secretase inhibitors target also other substrates besides APP and antibodies employed bind not only to APPsα, but also full-length APP and Aβ. Collectively, our findings indicate an important synaptotrophic role of APPsα in the mature CNS for spine density, synaptic plasticity, and behavior. Importantly, this role in cDKO mice (lacking endogenous APP and all its fragments including Aβ) is completely independent of any indirect Aβ related effects, in contrast to the previously reported Aβ lowering properties of APPsα in transgenic APP/PS1 mice (Obregon *et al*, 2012; Fol *et al*, 2016).

As APPsα and APPsβ are identical in primary sequence except for the last 16 amino acids, one may expect that they should exhibit largely overlapping functions. Accordingly, only few studies have so far directly compared the effects mediated by either APPsα or APPsβ. *In vitro*, recombinant APPsβ was shown to more efficiently induce the differentiation of human embryonic stem cells into neuronal precursor cells as compared to APPsα (Freude *et al*, 2011), whereas a similar increase in axonal outgrowth was observed when cortical neurons were treated with recombinant APPsβ or APPsα (Chasseigneaux *et al*, 2011). With regard to *in vitro* assays of neuroprotection, however, APPsβ was considerably less potent to protect neurons against glucose deprivation, excitotoxicity, Aβ peptide (Furukawa *et al*, 1996; Barger & Harmon, 1997), or epoxomicin-induced proteasomal stress (Copanaki *et al*, 2010).

Here, we compared the *in vivo* functions of the secreted APP ectodomains in the adult brain. A surprising key finding was that APPsα and APPsβ exert strikingly different effects *in vivo*, despite a similar level and pattern of AAV-mediated expression (Figs 1, 5C–E, EV1, and EV2). Of note, the absence of beneficial effects by AAV-APPsβ cannot be simply explained by possible adverse effects associated with AAV-APPsβ expression, as we found no signs of increased cell death, nor any evidence for increased astrogliosis or microgliosis (see Appendix Fig S1) as unspecific signs of neurodegeneration. Although earlier studies had indicated that a fragment (N-APPs1-286) derived for APPsβ may induce caspase activation and death of sensory neurons in a mechanism requiring DR6 (Nikolaev *et al*, 2009), these data have recently been revised to exclude a requirement for β-secretase activity and thus APPsβ (Olsen *et al*, 2014). Our notion that AAV-APPsβ does not induce adverse effects is further in agreement with previous data from fully viable and apparently normal APPsβ-knockin (KI) mice expressing solely APPsβ on an APLP2 wildtype background (Li *et al*, 2010). However, whether a lack of APPsα in APPsβ-KI mice might lead to synaptic deficits had remained unknown.

We demonstrate that APPsα but not APPsβ rescues spine density and synaptic plasticity in cDKO mice and identified the CTα16 peptide of APPsα as a crucial LTP-enhancing functional domain that stimulated LTP to the same extent as recAPPsα. Mechanistically, facilitation of LTP by APPsα or the CTα16 peptide required functional α7-nAChRs since BTX, a selective antagonist of α7-nAChRs, blocked its effects. Moreover, when expressed in oocytes α7-nAChRs could be directly potentiated by nanomolar amounts of either recAPPsα (but not recAPPsβ) or CTα16 in the presence of ACh or nicotine. Together with the ability of APPsα to enhance the sensitivity of α7-nAChRs for the agonist nicotine, these data establish APPsα as a potent positive allosteric modulator (PAM). These findings also suggest that APPsα might function as an endogenous PAM of cholinergic signaling in the hippocampus, although further studies are required to confirm its activity *in vivo*. Several studies have shown that nAChR activation facilitates LTP induction (for review see Yakel, 2014) and α7-nAChRs are abundantly expressed in the hippocampus (Fabian-Fine *et al*, 2001). Several mechanisms of α7-nAChR signaling are thought to contribute to its role in LTP: (i) Activation of presynaptic α7-nAChR can increase glutamate release and (ii) activation of postsynaptic α7-nAChRs that have a high Ca^{2+} permeability may confer membrane depolarization and induce plasticity evoking Ca^{2+} signaling (reviewed by McKay *et al*, 2007; Yakel, 2014).

Although more work is needed to understand precisely how APPsα affects α7-nAChR signaling, we hypothesize that both pre- and postsynaptic mechanisms are likely to play a role. When applied to slices of cDKO mice, both APPsα and CTα16 enhanced, in a BTX-sensitive manner, the early phase of post-tetanic potentiation (PTP) during the first minutes after start of baseline recording, which is believed to involve Ca^{2+} build up in presynaptic terminals. In line with an important endogenous role of APPsα for LTP, APPsα secretion is activity dependent (Fazeli *et al*, 1994; Mills & Reiner, 1999; Gakhar-Koppole *et al*, 2008; Hoey *et al*, 2009) and can thus be increased through plasticity-inducing protocols. The enhancement of PTP by APPsα, as observed in our study, is consistent with previous studies that reported increased Ca^{2+} influx in synaptoneurosomes and α7-nAChRs transfected neuroblastoma cells upon application of low (picomolar) amounts of Aβ or N-terminal Aβ-peptides that are overlapping with the C-terminus of APPsα (Dougherty *et al*, 2003; Lawrence *et al*, 2014). Recently, low (picomolar) amounts of Aβ were shown to increase synaptic vesicle recycling via α7-nAChRs signaling in hippocampal neurons (Lazarevic *et al*, 2017). Moreover, low amounts of Aβ had been found to stimulate synaptic plasticity and memory in wild-type mice (Puzzo *et al*, 2011; Lawrence *et al*, 2014). In addition to presynaptic effects, it is likely that APPsα will also modulate signaling at the postsynaptic site (for a review, see Ludewig & Korte, 2016). Postsynaptic membrane depolarization due to Ca^{2+} influx through α7-nAChRs may increase the probability of NMDAR activation that is crucial to induce stable LTP. In this regard, NMDAR inhibition has been shown to prevent the nicotine-induced conversion of short-term plasticity into LTP at CA3/CA1 synapses (Ji *et al*, 2001). Moreover, also activation of septal cholinergic input to induce α7-nAChRs-dependent LTP required the activation of NMDARs (Gu & Yakel, 2011). In addition to signaling via α7-nAChRs, APPsα may also modulate NMDARs more directly, as APPsα was shown to potentiate tetanically evoked NMDAR currents recorded at granule cells of the dentate gyrus in rat brain slices (Taylor *et al*, 2008) and full-length APP can biochemically interact with GluN1/GluN2 receptors (Cousins *et al*, 2009), although it is not known whether this also holds true for APPsα.

Our findings of distinct *in vivo* functions of APPsα and APPsβ have important implications for AD therapy. Pharmacological BACE1 inhibition has been a major approach to reduce Aβ in animals and clinical trials. More recently, however, concerns have been raised that therapeutic BACE1 inhibition may also compromise important physiological functions of BACE (Yan & Vassar, 2014). Indeed, BACE-KO mice display deficits in synaptic morphology and synaptic plasticity in the hippocampus (Dominguez *et al*, 2005; Laird *et al*, 2005). Our data indicate that APPsβ deficiency that will result from BACE1 inhibition is unlikely to lead to toxic effects. A number of recent studies demonstrated that very low concentrations of Aβ may stimulate transmitter release and modulate synaptic plasticity and memory. Strikingly, we now show that it is the C-terminal domain of APPsα that is required to increase spine density, rescues LTP, and improves memory. As this C-terminal domain is also present in Aβ, it is conceivable that signaling of APPsα and soluble, non-aggregated Aβ species may at least in part converge, for example, regarding the activation of α7-nAChRs. From this, one may speculate that APPsα may be able to rescue potential unwanted effects due to limited Aβ levels. It is also clear, however, that

sequence context and structural accessibility of the CTα16 domain is crucial. Indeed, the presence of the CTα16 domain appears to alter the conformation of APPsα in a critical way. Analysis by small-angle X-ray diffraction indicated that the 3D structure of APPsα and APPsβ is quite different, with APPsα exhibiting an extended conformation with an exposed CTα16 region (Gralle *et al*, 2006; Peters-Libeu *et al*, 2015), while in APPsβ the E1 domain folds back towards the C-terminal juxtamembrane region (Peters-Libeu *et al*, 2015). Thus, different 3D structures may enable or prevent binding to receptors, which may contribute to the distinct *in vivo* functions of APPsα and APPsβ.

Regarding AD pathogenesis, our data indicate that a shift towards β-secretase processing that may occur during AD (Holsinger *et al*, 2002; Ahmed *et al*, 2010) could result in insufficient amounts of APPsα that cannot be functionally compensated by APPsβ. A lack or reduction of APPsα might thus contribute to deficits in synaptic plasticity and cognitive function in AD patients. Consistent with this notion, in AD patients hippocampal levels of synaptically localized ADAM10/SAP97 complexes are reduced (Epis *et al*, 2010) and an activity attenuating mutation in the human ADAM10 gene leading to reduced APPsα levels has been associated with AD (Kim *et al*, 2009; Suh *et al*, 2013). In familial AD cases carrying the Swedish mutation (APP_{SWE}), cerebrospinal fluid (CSF) levels of APPsα were found to be reduced already at early stages of AD (Lannfelt *et al*, 1995; Almkvist *et al*, 1997). With regard to sporadic AD cases, however, no consensus has been reached whether reduced APPsα levels are associated with AD (Mockett *et al*, 2017). Early on, total soluble APPs was reported to be severely reduced in sporadic AD (Van Nostrand *et al*, 1992). Several more recent studies specifically detecting APPsα reported reduced APPsα levels in mild (Sennvik *et al*, 2000) to moderate AD (Rosen *et al*, 2012), or in APOE4-positive AD patients (Olsson *et al*, 2003), while several other studies found no difference in APPsα at early stages of sporadic AD (Perneczky *et al*, 2011, 2013; Rosen *et al*, 2012; Brinkmalm *et al*, 2013). These mixed results may in part be related to different assays systems used and the recent finding of considerable diurnal variability of APPsα and other APP fragments in the CSF (Dobrowolska *et al*, 2014). Thus, more detailed studies are needed to resolve these important issues.

In preclinical AD research, numerous studies have been conducted using APP transgenic mouse models (https://www.alzforum.org/research-models) which (over)express $huAPP_{SWE}$ that undergoes enhanced β-secretase processing. Consequently, reduced levels of neuroprotective and synaptotrophic APPsα relative to increased amounts of Aβ (that is a reduced APPsα/Aβ ratio) may fail to adequately balance and antagonize the detrimental effects of Aβ and thus contribute to the phenotypic and synaptic impairments in these transgenic mice.

APPsα also plays an important role in processes of natural aging. Not only is memory performance correlated with APPsα levels in rats (Anderson *et al*, 1999), but also aging-related deficits in LTP and cognitive behavior can be rescued by exogenous APPsα (Moreno *et al*, 2015; Xiong *et al*, 2016). Collectively, our findings indicate distinct functions for APPsα in the adult brain to modulate spine density, synaptic plasticity, and cognition. Our findings lend further support to therapeutic approaches aimed at directly or indirectly increasing APPsα expression in the brain (Mockett *et al*, 2017; Müller *et al*, 2017) to ameliorate synaptic deficits in AD or possibly also for other diseases in which neurons are damaged.

Materials and Methods

Mice

Experiments on animals were performed in accordance with the guidelines and regulations set forth by the German Animal Welfare Act, the Regierungspräsidium Karlsruhe (Germany) and the Regierungspräsidium Darmstadt (Germany). Generation and genotyping of NexCre cDKO mice (further referred as cDKO mice) were as described previously (Hick *et al*, 2015). Genotype of experimental animals: NexCre cDKO (=$APP^{flox/flox}$ $APLP2^{-/-}$ $NexCre^{+}$) and Cre^{-} littermate (LM) controls (=$APP^{flox/flox}$ $APLP2^{-/-}$).

AAV plasmid design and vector production

The mouse APPsα coding sequence (derived from Uniprot: P12023-2) was codon optimized (Geneart, Germany) and then cloned under control of the synapsin promoter into a single-stranded rAAV2-based shuttle vector, as described previously (Fol *et al*, 2016). Briefly, the bicistronic DNA constructs harbor a T2A site that connects the cDNA of lckVenus and muAPPsα. Venus contains a lymphocyte-specific protein tyrosine kinase (lck)-derived peptide motif which tethers it to the plasma membrane. For easy detection, an N-terminal double HA-tag was inserted downstream of the APP signal peptide (SP) at the N-terminus of APPsα. The monocistronic control vector, AAV-Venus, encodes only the yellow fluorescent protein Venus. All constructs were packaged into AAV9 capsids. Briefly, viral particles were produced by transient co-transfection of HEK-293 cells with the transfer vector containing the above-mentioned expression cassettes and the helper plasmid pDP9rs. 72 h following transfection, virions were purified and concentrated from cell lysate and supernatant by ultracentrifugation on a iodixanol density gradient followed by buffer exchange to 0.01% pluronic/phosphate-buffered saline (PBS) via a 100 kDa Amicon centrifugal filter unit. Genome copies in the vector stocks were determined by free inverted terminal repeat (ITR)-specific quantitative TaqMan PCR and expressed as genomic copies per μl of concentrated stocks (gc/μl) as described (D'Costa *et al*, 2016).

Stereotactic injection of AAVs

Mice were anesthetized by intraperitoneal injection of sleep mix (Medetomedin: 500 μg/kg, Midazolam: 5 mg/kg, Fentanyl: 50 μg/kg in isotonic NaCl solution) and positioned on a stereotactic frame (World Precision Instruments, USA). Vector particles (either AAV-Venus, AAV-APPsα or AAV-APPsβ) were injected into the hippocampus at two injection spots per hemisphere using 1 μl vector stock (titer: 1×10^9 gc/μl) per spot at a rate of 0.2 μl/min. When injection was completed, the cannula was left to rest for 1 min to prevent efflux of viral vector solution. Stereotactic coordinates of injection sites from bregma were as follows: anteroposterior (A/P): −2 mm, mediolateral (M/L): ±1 mm, dorsoventral (D/V):

−2.25 mm and −1.75 mm. Procedures were approved by the local animal care and use committee (35-9185.81/G-304/14, Regierungspräsidium Karlsruhe, Germany).

Brain samples

Mice were sacrificed 6 weeks post-injection at 5–6 months of age. Following anesthesia, mice were transcardially perfused with PBS before dissection. For immunohistochemistry, one cerebral hemisphere was dissected and post-fixed in 4% paraformaldehyde (PFA) for 48 h and afterwards stored in PBS at 4°C. 40-μm coronal sections were cut using a vibratome (HM650V Vibratome, Thermo Fisher Scientific, USA) and collected in PBS. The other hemisphere was dissected to segregate hippocampus and cortex for biochemical analysis. Samples were then homogenized using a Polytron homogenizer (Polytron PT-MR 2100, Kinematica AG, Switzerland) in tissue homogenization buffer (THB, 250 mM sucrose, 1 mM EGTA, 20 mM Tris–HCl, pH 7.4) containing 1× protease inhibitor (Complete™ #04693124001, Roche, Switzerland). After centrifugation (10 min, 15,700 *g*, 4°C), the supernatant was collected and the protein concentration was quantified by BCA assay. Lysate aliquots were snap-frozen in liquid N_2 and stored at −80°C. For the detection of the soluble ectodomain fragments APPs, hippocampal lysates were subjected to high-speed centrifugation (60 min at 100,000 × *g*) and membrane-free supernatant was used for further analysis.

Western blot analysis

Total brain homogenate or supernatant from ultracentrifugation (10 μg protein) was used for SDS–PAGE. Proteins were separated using 12% Tris-Glycine gels at 20 mA/gel in Laemmli buffer (0.25 M Tris, 2 M glycine and 1% SDS) and transferred to 0.45 μm PVDF membranes (GE Healthcare, USA) using a tank blot at 450 mA for 1 h (for samples after ultracentrifugation: 450 mA for 1.5 h). After blocking in PBS-T (2.5% Tween in PBS) containing 5% (w/v) dried milk powder at room temperature for 60 min, membranes were incubated with the primary antibodies at 4°C overnight. The following antibodies were used: α-HA-tag (rabbit, 1:1,000, #3724, Cell Signaling Technology, USA, was used for total hippocampal homogenates or mouse, 1:1,000, #2367, Cell Signaling Technology, USA, used for analysis after ultracentrifugation), α-GFAP (rabbit, 1:3,000, #173002, Synaptic Systems, Germany), α-Iba1 (rabbit, 1:500, #234003, Synaptic Systems, Germany), α-GFP (chicken, 1:1,000, #A10262, Thermo Fisher Scientific, USA), anti-β-Tubulin (mouse, 1:10,000, #MAB3408, Merck Millipore, USA), M3.2 (mouse, 1:1,000, kind gift from Paul Mathews), Y188 (rabbit, 1:1,000, #ab32136, Abcam, UK). Membranes were then washed with PBS-T, incubated with a horseradish peroxidase-coupled secondary antibody (goat-α-mouse HRP, 1:10,000, #115-165-146, Dianova, Germany; donkey-α-rabbit HRP, 1:10,000, #711-035-152, Dianova, Germany; goat-α-chicken HRP, 1:10,000, #103-035-155, Dianova, Germany), and washed again and developed using SignalFire ECL Reagent (#6883, Cell Signaling Technology, USA) or SignalFire™ Elite ECL Reagent (used for analysis after ultracentrifugation, #12757, Cell Signaling Technology, USA). Signals were detected with the Bio-Rad Chemidoc MP imager (Bio-Rad, Hercules, USA) and analyzed using Bio-Rad Image Lab software.

Immunostaining

Slices were blocked/permeabilized in blocking buffer (5% BSA, 5% NGS, 0.4% Triton X-100 in PBS) overnight at 4°C. To detect AAV-encoded HA-tagged HA-APPsα, slices were incubated with α-HA antibody (rabbit-α-HA, 1:1,000, #3724, Cell Signaling Technology, USA or mouse-α-HA, 1:1,000, #H3667, Sigma-Aldrich, USA) overnight at 4°C. After three successive washes with PBS-T (2.5% Tween in PBS), slices were incubated in secondary antibody (goat-α-rabbit Cy3, 1:1,500, #711-165-152, Jackson ImmunoResearch Laboratories, USA; goat-α-rabbit Cy5, 1:1,500, #111-175-144, Jackson ImmunoResearch Laboratories, USA; donkey-α-mouse Cy3, 1:1,500, #715-165-150, Jackson ImmunoResearch Laboratories, USA; goat-α-mouse Cy5, 1:1,500, #A10524, Thermo Fisher Scientific, USA). For expression analysis, HA-APPsα was coimmunostained overnight with the following primary antibodies: α-NeuN (mouse, 1:1,500, #MAB377, Merck Millipore, USA), α-GFAP (rabbit, 1:3,000, #173002, Synaptic Systems, Germany), and α-Iba1 (rabbit, 1:500, #234003, Synaptic Systems, Germany). Images were taken with a Axio Observer Z1 (Zeiss, Germany) and a Leica TCS SP5II (Leica, Germany).

Electrophysiology

In vitro extracellular recordings were performed on acute hippocampal slices of LM controls stereotactically injected with the AAV-Venus ($N = 5$) and cDKO mice injected either with AAV-Venus ($N = 4$) or AAV-APPsα ($N = 5$). In a separate set of experiments, cDKO mice were injected either with AAV-Venus ($N = 5$) or AAV-APPsβ ($N = 5$). Investigation of synaptic plasticity was done 7–8 weeks after AAV injection. In-between animals were housed in a temperature- and humidity-controlled room with a 12 h light–dark cycle and had access to food and water *ad libitum*.

Slice preparation

Acute hippocampal transversal slices were prepared from isoflurane anesthetized individuals. Following decapitation, the brain was removed and quickly transferred into ice-cold carbogenated (95% O_2, 5% CO_2) artificial cerebrospinal fluid (ACSF) containing 125.0 mM NaCl, 2.0 mM KCl, 1.25 mM NaH_2PO_4, 2.0 mM $MgCl_2$, 26.0 mM $NaHCO_3$, 2.0 mM $CaCl_2$, and 25.0 mM glucose. The hippocampus was sectioned into 400-μm-thick transversal slices with a vibrating microtome (VT1200S, Leica, Germany) and maintained in carbogenated ACSF at room temperature for at least 1.5 h. Before recording, each slice of the injected animals was inspected for Venus expression in area CA1 and CA3 (Axiovert 35, Zeiss). Slices lacking fluorescence in the recording areas were excluded from further analysis.

Peptides and inhibitor

Acute hippocampal slices of LM controls and cDKO mice were preincubated in 30 ml gently carbogenated ACSF containing synthetic CTα16 (DAEFGHDSGFEVRHQK) or a scrambled $CT\alpha16_{scr}$ peptide (RFDQHGVEDHAFGESK) of the same amino acid composition as a control. Recombinant recAPPsα was purified from the supernatant of stably transfected HEK cells as described (Hick *et al*, 2015) and was used at a concentration of 10 nM, in a custom-made incubation chamber for 1 h at RT. Afterwards slices were transferred into the

recording chamber where again 30 ml of ACSF with the respective peptide was circulating in a closed loop during the entire experiment. In another set of experiments, the α7-nicotinic acetylcholine receptor antagonist (α7-nAChR) α-Bungarotoxin (BTX, Merck Millipore, Germany) solved in *Aqua dest.* was used at a final concentration of 10 nM and either co-applied already at the step of pre-incubation (1 h before TBS) together with 10 nM CTα16 (or 10 nM APPsα) on acute slices or washed in 10 min before baseline recording started.

Extracellular field recordings

Slices were placed in a submerged recording chamber and perfused with carbogenated ACSF (32°C, 125.0 mM NaCl, 2.0 mM KCl, 1.25 mM NaH_2PO_4, 2.0 mM $MgCl_2$, 26.0 mM $NaHCO_3$, 2.0 mM $CaCl_2$, and 25.0 mM glucose) at a rate of 1.2–1.5 ml/min. Field excitatory postsynaptic potentials (*f*EPSPs) were recorded in stratum radiatum of CA1 region with a borosilicate glass micropipette (resistance 2–4 MΩ) filled with 3 M NaCl at a depth of ~ 150–200 μm. Monopolar tungsten electrodes were used for stimulating the Schaffer collaterals at a frequency of 0.1 Hz. Stimulation intensity was adjusted to ~ 40% of maximum *f*EPSP slope for 20 min baseline recording. LTP was induced by applying theta burst stimulation (TBS: 10 trains of four pulses at 100 Hz in an 200 ms interval, repeated three times).

Basal synaptic transmission properties were analyzed via input–output (IO) measurements, and short-term plasticity was examined via PPF. The IO measurements were performed either by application of defined current values (25–250 μA) or by adjusting the stimulus intensity to certain fiber volley (FV) amplitudes (0.1–0.8 mV). Presynaptic function and short-term plasticity were assessed with the PPF paradigm by applying a pair of two closely spaced stimuli in inter-stimulus intervals (ISI) ranging from 10 to 160 ms.

Data analysis and statistics

Data of electrophysiological recordings were collected, stored, and analyzed with LABVIEW software (National Instruments, USA). The initial slope of *f*EPSPs elicited by stimulation of the Schaffer collaterals was measured over time, normalized to baseline, and plotted as average ± SEM. Analysis of the PPF data was performed by calculating the ratio of the slope of the second *f*EPSP divided by the slope of the first one and multiplied by 100. The statistical analysis was performed using Microsoft Excel or GraphPad Prism version 6.0 (GraphPad, USA). Data obtained between two genotypes or two different experimental conditions were compared using an unpaired two-tailed Student's *t*-test. Data including more than two different groups were analyzed using a one-way ANOVA followed by a *post hoc* Bonferroni's test. All data are indicated as mean ± SEM. Values of $P < 0.05$ were considered significant and plotted as follows $^*P < 0.05$, $^{**}P < 0.01$, $^{***}P < 0.001$.

Xenopus *oocyte expression and electrophysiological recording*

The rat α7-nAChR, kindly provided by A. Nicke (Kendel *et al*, 2013), and the human α1-GlyR (Laube *et al*, 2000) cDNAs were subcloned into the oocyte expression vector pNKS2. The original rat α7-nAChR cDNA had been provided by J. Patrick (Baylor College of Medicine, Houston, USA). The rat α7-nAChR or the human α1-GlyR cDNA was linearized, and cRNA was synthesized with the SP6 or T7 mMessage mMachine kit, respectively (Ambion, USA). For electrophysiological analysis, *X. laevis* oocytes were injected with 50 ng of the cRNA in a volume of 50 nl. Oocytes were isolated and maintained as described previously (Laube *et al*, 1997) and approved by the local animal care and use committee (II25.3-19c20/15, RP Darmstadt, Germany). 1–3 days after injection, whole-cell currents were recorded at −70 mV by two-electrode voltage clamp according to Laube *et al* (2000). Currents were acquired at 200 Hz with a Geneclamp 500B amplifier, a Digidata 1322A digitizer, and Clampex 9.2 software (Molecular Devices, USA). The agonists nicotine, acetylcholine, or glycine, dissolved in bath solution, was applied either alone for 10 s or after 15 s pre-application of the respective peptides (CTα16, $CT\alpha16_{scr}$, recAPPsα, or recAPPsβ) also dissolved in bath solution. All experiments were performed at room temperature.

Data analysis and statistics

Currents were measured with Clampfit 9.2 software (Molecular Devices, USA), and results were analyzed using the KaleidaGraph program (Synergy Software, USA) and GraphPad Prism version 6.0 (GraphPad, USA). Peak current responses to nicotine in the absence or presence of APPsα were plotted against agonist concentration and fit with variable slope nonlinear regression to establish agonist EC_{50} parameter (Laube *et al*, 2000). For peptide modulation, responses to EC_{50} nicotine (100 μM), acetylcholine (100 μM), or glycine (100 μM) after application were analyzed. Normalized CTα16-induced fold enhancement of nicotine-induced currents was fit with variable slope nonlinear regression (GraphPad Prism version 6.0, GraphPad, USA), yielding EC_{50} parameters for each individual experiment (Laube *et al*, 1998). All experiments were from at least two batches of oocytes. Data were compared by paired two-tailed Student's *t*-test. Values of $P < 0.05$ were considered significant and plotted as follows $^*P < 0.05$, $^{**}P < 0.01$, $^{***}P < 0.001$. All data are indicated as mean ± SEM.

Neuronal morphology and spine density

Iontophoretic fillings

In brief, CA1 pyramidal cells were visualized by postfixation filling with Alexa 568 in 200-μm horizontal brain sections of 5- to 6-month-old mice (see Appendix Table S1 for sex of animals). For iontophoretic fillings of CA1 pyramidal neurons, one brain slice at a time was placed in a custom-made chamber filled with cold PBS and visualized on an Olympus BX51WI fixed stage upright microscope (Olympus, Japan). Sharp quartz glass electrodes (Quartz electrodes with filament, O.D: 1.0 mm, I.D.: 0.7 mm, 10 cm length, Sutter instruments, USA) were pulled using the Sutter P-2000 Laser Puller. The tip of the electrode was loaded with 5 mM Alexa 568 dye dissolved in distilled water and backfilled with 0.1 M LiCl dissolved in distilled water. Using a motorized 3D micromanipulator, the electrode was lowered into the hippocampal CA1 region under visual control using a Calcium Crimson filter cube (HQ580/20×, U-Q595LP (339038), HQ630/60 m) while applying a negative voltage pulse (−1 V, 1 Hz) to the electrode via a silver wire in line with a 500 MΩ resistor. When piercing of a cell body was observed, the cell was filled by application of a negative 1 Hz current pulse (~ 5 nA) to the electrode. Filling was for 10 min or until no further filling was observed. Afterwards slices were fixed for 2 days in 4% PFA at 4°C, washed three times in cold PBS, and finally mounted in Mowiol.

Image acquisition

Images of filled neurons were acquired on a Leica TCS SP5II (Leica, Germany) upright confocal microscope. Overview images of complete neurons used for reconstruction were taken with a 20× objective (Apo 20×/0.75). The complete volume of one filled neuron was imaged with a *z*-step size of 1 μm and a 2,048 × 2,048 resolution. Basal and apical segments were imaged individually with two overlapping stacks. Detailed images of dendritic segments and spines were acquired using a 63× objective (Apo 63×/1.4 oil) and a digital zoom of 5. To fulfill the Nyquist criteria for deconvolution, *z*-stacks of dendritic segments were captured with a pixel size of 80 nm and a *z*-step of 130 nm. Laserpower, gain and offset varied from cell to cell as the parameters were always chosen so that the complete range of the grayscale was used. Images for spine counts were deconvoluted with the AutoQuantX3 software (Media Cybernetics, USA).

Neuronal morphology and spine counts

Filled CA1 pyramidal neurons were manually reconstructed using the Neurolucida software (MicroBrightField, USA) by an experimentator blind to genotype and injected viral vector. Neurons were only included into Sholl analysis if they showed a completely filled apical or basal tree and well-defined dendritic endings. The morphometric Sholl analysis was done using the NeuroExplorer software (MicroBrightField, USA). In short, a series of concentric spheres (centered around the soma) was drawn with an intersection interval of 30 μm and the number of dendrites crossing each sphere, as well as the dendritic length in between each sphere was calculated. This analysis was done separately for basal and apical dendrites and was plotted against the distance from the soma. For evaluation of basal dendritic spine density, at least three different randomly chosen dendritic segments of the basal dendritic arbor were imaged. They had to fulfill the following criteria: (i) lie mostly horizontally to the slice surface, (ii) be at least 20 μm away from the soma, (iii) have a comparable thickness. The minimum basal dendritic length imaged per neuron was 100 μm. For evaluation of midapical dendritic spine density, at least three different dendritic segments of the apical tree were imaged. Midapical was defined as the middle third of the length of the apical dendrite measured from the origin of the apical dendrite from the soma to the endpoint of the tufts. Dendritic segments used for evaluation had to fulfill the following criteria: (i) be of second or third order to assure comparable shaft thickness, (ii) lie in the middle third of the main apical dendrite, (iii) be longer than 10 μm. The minimum midapical dendritic length imaged per neuron was 100 μm. Files in the ND2 format were imported into ImageJ (NIH) using the BioFormats Importer. After adjusting, images were saved in the TIFF format. Dendritic spines were manually counted using the Neurolucida and NeuroExplorer software (MicroBrightField, USA) following the criteria of Holtmaat (Holtmaat *et al*, 2009) with minor modifications: (i) All spines that protruded laterally from the dendritic shaft and exceeded a length of 0.4 μm were counted. (ii) Spines that protruded into the *z*-plane were only counted if they exceeded the dendritic shaft more than 0.4 μm to the lateral side. (iii) Spines that bisected were counted as two spines. (iv) Spines had to be at least 10 μm away from branching points and the soma. Spine density was expressed as spines per μm of dendrite. Prior to statistical analysis and blind to genotype, neurons were excluded if the image quality (poor signal to noise ratio) was not sufficient for counting of spines or for deconvolution.

Golgi staining

Golgi staining was done using the Rapid Golgi Staining Kit (FD NeuroTechnologies, USA) according to the manufacturer's instructions. All procedures were performed under dark conditions. One hemisphere of each mouse was used for Western blot analysis and the other hemisphere for Golgi staining (see Appendix Table S1 for sex of animals). Hemispheres were immersed in 2.5 ml mixtures of equal parts of kit solutions A and B and incubated at room temperature for 2 weeks. After 24 h solution (A + B) was renewed. Afterwards brain tissues were stored in solution C at 4°C for at least 72 h, once exchanged after 24 h. Brains were snap-frozen on dry ice, and coronal sections of 100 μm were cut with a cryotome (Hyrax C50, Zeiss). Each section was mounted with Solution C on an adhesive microscope slide pre-coated with 1% gelatin/0.1% chrome alum on both sides and stained according to the manufacturer's protocol with the exception that RotiClear (Roth, Germany) was used instead of xylene. Finally, slices were cover-slipped with Permount (Thermo Fisher Scientific, USA).

Imaging and analysis of spine density after Golgi staining

Imaging of second- or third-order dendritic branches of hippocampal pyramidal neurons of area CA1 was done with an Axio Observer Z1 (Zeiss) for Golgi-stained neurons using a 63× oil objective. *Z*-stack thickness was held constant at 130 nm. The number of spines was determined per micrometer of dendritic length (in total 100 μm per neuron) at apical and basal compartments using Neurolucida software (MicroBrightField, USA). Spines in the area around branching points and the soma were excluded from analysis. Five animals per genotype and 3–4 neurons per animal were analyzed blind to genotype and injected viral vector.

Behavioral analysis

Animals

Mice (cDKO + AAV-APPsα: 9M + 9F, cDKO + AAV-Venus: 8M + 10F, LM control + AAV-Venus: 12M + 10F) were housed under a 12/12 h light–dark cycle (lights on at 20:00) in groups of 2–5, unless individual housing was required by experimental protocols or to prevent fighting. Testing occurred during the dark phase under dim light (approximately 12 lux). Mice were transferred to the testing room 30 min before testing. Procedures were approved by the Veterinary Office of the Kanton of Zurich (license 44/2015).

Behavioral procedures

Morris water maze place navigation. The round white polypropylene pool had a diameter of 150 cm with 68 cm high walls. It was filled with water (24–26°C, depth 15 cm) and rendered opaque by addition of 1 l of milk (UHT whole milk 3.5% fat, Coop, Switzerland). The white quadratic goal platform (14 × 14 cm) was made of metallic wire mesh. It was hidden 0.5 cm below the water surface in the center of one of the four quadrants, 30 cm from the side wall. Salient extra-maze cues were placed on the walls of the testing room. Animals performed 30 training trials (max. duration 120 s), 6 per day with intertrial intervals of 30–60 min and varying starting positions. During the first 18 trials, the hidden platform was held in

the same position (acquisition phase) and then moved to the opposite quadrant for the remaining 12 trials (reversal phase). The first 60 s of the first reversal trial served as probe trial to test for spatial retention. Time spent in a circular target zone comprising 12.5% of the pool surface was compared with corresponding control zones in adjacent quadrants.

Data analysis and statistics

The path of moving mice was tracked using Noldus EthoVision 3.1 (Noldus, Netherlands). For analysis, all data were imported in custom programmed software Wintrack (www.wintrack.ch; Wolfer *et al*, 2001). Data were evaluated using an ANOVA model with genotype (cDKO + AAV-APPsα, cDKO + AAV-Venus, LM control + AAV-Venus) and sex as between subject factors. Within subject factors were added as needed to explore the dependence of genotype effects on place or time. Significant interactions and where necessary significant main effects were further explored by pairwise *t*-tests or by splitting the ANOVA model, as appropriate. Variables with strongly skewed distributions or strong correlations between variances and group means were subjected to Box-Cox transformation before statistical analysis. The significance threshold was set at 0.05. The false discovery rate (FDR) control procedure of Hochberg was applied to groups of conceptually related variables within single tests to correct significance thresholds for multiple comparisons. Similarly, FDR correction was applied during *post hoc* testing. As genotype and treatment effects were independent of sex, the sex factor is not reported in results and figures. Statistical analyses were run using R version 3.2.3 complemented with the packages psych and moments.

For further methods related to EV Figures, see Appendix Supplementary Methods.

Expanded View for this article is available online.

Acknowledgements

We acknowledge funding by the Deutsche Forschungsgemeinschaft FOR1332 to MK and UM (MU1457/8-2, MU1457/9-2 and MU1457/14-1 to UM and KO1674/3-2 to MK) and by the Else-Kröner Fresenius-Stiftung (2014-A229 to UM). DPW is a member of the of the Neuroscience Center Zurich (ZNZ) and of the Zurich Center for Integrative Human Physiology (ZIHP). We thank Annette Nicke for providing the plasmid encoding the α7-nAChR cDNA.

Author contributions

UCM designed and conceived the study. MCR, SK, and SW performed intracranial AAV injections and analyzed data. CB and KH produced recombinant APPs. MCR performed and analyzed experiments related to APPs expression analysis *in vitro* and *in vivo* including Western blots, and performed immunochemistry and Sholl analysis including spine density measurements. SL, LRS, and MK performed extracellular electrophysiological recordings in brain slices, analyzed data, and interpreted results. AW and BL performed electrophysiological recordings in oocytes, analyzed data, and interpreted results. TA and CJB generated AAV vectors and analyzed APPs expression in neurons. A-KF and DPW conducted, analyzed, and interpreted behavioral experiments. UCM wrote the manuscript with help from MCR and input from all authors.

Conflict of interest

The authors declare that they have no conflict of interest.

References

Ahmed RR, Holler CJ, Webb RL, Li F, Beckett TL, Murphy MP (2010) BACE1 and BACE2 enzymatic activities in Alzheimer's disease. *J Neurochem* 112: 1045 – 1053

Almkvist O, Basun H, Wagner SL, Rowe BA, Wahlund LO, Lannfelt L (1997) Cerebrospinal fluid levels of alpha-secretase-cleaved soluble amyloid precursor protein mirror cognition in a Swedish family with Alzheimer disease and a gene mutation. *Arch Neurol* 54: 641 – 644

Anderson JJ, Holtz G, Baskin PP, Wang R, Mazzarelli L, Wagner SL, Menzaghi F (1999) Reduced cerebrospinal fluid levels of alpha-secretase-cleaved amyloid precursor protein in aged rats: correlation with spatial memory deficits. *Neuroscience* 93: 1409 – 1420

Barger SW, Harmon AD (1997) Microglial activation by Alzheimer amyloid precursor protein and modulation by apolipoprotein E. *Nature* 388: 878 – 881

Brinkmalm G, Brinkmalm A, Bourgeois P, Persson R, Hansson O, Portelius E, Mercken M, Andreasson U, Parent S, Lipari F, Ohrfelt A, Bjerke M, Minthon L, Zetterberg H, Blennow K, Nutu M (2013) Soluble amyloid precursor protein alpha and beta in CSF in Alzheimer's disease. *Brain Res* 1513: 117 – 126

Chasseigneaux S, Dinc L, Rose C, Chabret C, Coulpier F, Topilko P, Mauger G, Allinquant B (2011) Secreted amyloid precursor protein beta and secreted amyloid precursor protein alpha induce axon outgrowth *in vitro* through Egr1 signaling pathway. *PLoS One* 6: e16301

Chasseigneaux S, Allinquant B (2012) Functions of Abeta, sAPPalpha and sAPPbeta: similarities and differences. *J Neurochem* 120(Suppl 1): 99 – 108

Copanaki E, Chang S, Vlachos A, Tschape JA, Muller UC, Kogel D, Deller T (2010) sAPPalpha antagonizes dendritic degeneration and neuron death triggered by proteasomal stress. *Mol Cell Neurosci* 44: 386 – 393

Cousins SL, Hoey SE, Anne Stephenson F, Perkinton MS (2009) Amyloid precursor protein 695 associates with assembled NR2A- and NR2B-containing NMDA receptors to result in the enhancement of their cell surface delivery. *J Neurochem* 111: 1501 – 1513

Dawson GR, Seabrook GR, Zheng H, Smith DW, Graham S, O'Dowd G, Bowery BJ, Boyce S, Trumbauer ME, Chen HY, Van der Ploeg LH, Sirinathsinghji DJ (1999) Age-related cognitive deficits, impaired long-term potentiation and reduction in synaptic marker density in mice lacking the beta-amyloid precursor protein. *Neuroscience* 90: 1 – 13

D'Costa S, Blouin V, Broucque F, Penaud-Budloo M, Francois A, Perez IC, Le Bec C, Moullier P, Snyder RO, Ayuso E (2016) Practical utilization of recombinant AAV vector reference standards: focus on vector genomes titration by free ITR qPCR. *Mol Ther Methods Clin Dev* 5: 16019

Dobrowolska JA, Kasten T, Huang Y, Benzinger TL, Sigurdson W, Ovod V, Morris JC, Bateman RJ (2014) Diurnal patterns of soluble amyloid precursor protein metabolites in the human central nervous system. *PLoS One* 9: e89998

Dominguez D, Tournoy J, Hartmann D, Huth T, Cryns K, Deforce S, Serneels L, Camacho IE, Marjaux E, Craessaerts K, Roebroek AJ, Schwake M, D'Hooge R, Bach P, Kalinke U, Moechars D, Alzheimer C, Reiss K, Saftig P, De Strooper B (2005) Phenotypic and biochemical analyses of BACE1- and BACE2-deficient mice. *J Biol Chem* 280: 30797 – 30806

Dougherty JJ, Wu J, Nichols RA (2003) Beta-amyloid regulation of presynaptic nicotinic receptors in rat hippocampus and neocortex. *J Neurosci* 23: 6740 – 6747

Epis R, Marcello E, Gardoni F, Vastagh C, Malinverno M, Balducci C, Colombo A, Borroni B, Vara H, Dell'Agli M, Cattabeni F, Giustetto M, Borsello T,

Forloni G, Padovani A, Di Luca M (2010) Blocking ADAM10 synaptic trafficking generates a model of sporadic Alzheimer's disease. *Brain* 133: 3323 – 3335

Fabian-Fine R, Skehel P, Errington ML, Davies HA, Sher E, Stewart MG, Fine A (2001) Ultrastructural distribution of the alpha7 nicotinic acetylcholine receptor subunit in rat hippocampus. *J Neurosci* 21: 7993 – 8003

Fazeli MS, Breen K, Errington ML, Bliss TV (1994) Increase in extracellular NCAM and amyloid precursor protein following induction of long-term potentiation in the dentate gyrus of anaesthetized rats. *Neurosci Lett* 169: 77 – 80

Fol R, Braudeau J, Ludewig S, Abel T, Weyer SW, Roederer JP, Brod F, Audrain M, Bemelmans AP, Buchholz CJ, Korte M, Cartier N, Muller UC (2016) Viral gene transfer of APPsalpha rescues synaptic failure in an Alzheimer's disease mouse model. *Acta Neuropathol* 131: 247 – 266

Freude KK, Penjwini M, Davis JL, LaFerla FM, Blurton-Jones M (2011) Soluble amyloid precursor protein induces rapid neural differentiation of human embryonic stem cells. *J Biol Chem* 286: 24264 – 24274

Furukawa K, Sopher BL, Rydel RE, Begley JG, Pham DG, Martin GM, Fox M, Mattson MP (1996) Increased activity-regulating and neuroprotective efficacy of alpha-secretase-derived secreted amyloid precursor protein conferred by a C-terminal heparin-binding domain. *J Neurochem* 67: 1882 – 1896

Gakhar-Koppole N, Hundeshagen P, Mandl C, Weyer SW, Allinquant B, Muller U, Ciccolini F (2008) Activity requires soluble amyloid precursor protein alpha to promote neurite outgrowth in neural stem cell-derived neurons via activation of the MAPK pathway. *Eur J Neurosci* 28: 871 – 882

Gralle M, Oliveira CL, Guerreiro LH, McKinstry WJ, Galatis D, Masters CL, Cappai R, Parker MW, Ramos CH, Torriani I, Ferreira ST (2006) Solution conformation and heparin-induced dimerization of the full-length extracellular domain of the human amyloid precursor protein. *J Mol Biol* 357: 493 – 508

Gu Z, Yakel JL (2011) Timing-dependent septal cholinergic induction of dynamic hippocampal synaptic plasticity. *Neuron* 71: 155 – 165

Hales JB, Schlesiger MI, Leutgeb JK, Squire LR, Leutgeb S, Clark RE (2014) Medial entorhinal cortex lesions only partially disrupt hippocampal place cells and hippocampus-dependent place memory. *Cell Rep* 9: 893 – 901

Heber S, Herms J, Gajic V, Hainfellner J, Aguzzi A, Rulicke T, von Kretzschmar H, von Koch C, Sisodia S, Tremml P, Lipp HP, Wolfer DP, Muller U (2000) Mice with combined gene knock-outs reveal essential and partially redundant functions of amyloid precursor protein family members. *J Neurosci* 20: 7951 – 7963

Hefter D, Kaiser M, Weyer SW, Papageorgiou IE, Both M, Kann O, Muller UC, Draguhn A (2016) Amyloid precursor protein protects neuronal network function after hypoxia via control of voltage-gated calcium channels. *J Neurosci* 36: 8356 – 8371

Hick M, Herrmann U, Weyer SW, Mallm JP, Tschape JA, Borgers M, Mercken M, Roth FC, Draguhn A, Slomianka L, Wolfer DP, Korte M, Muller UC (2015) Acute function of secreted amyloid precursor protein fragment APPsalpha in synaptic plasticity. *Acta Neuropathol* 129: 21 – 37

Hoey SE, Williams RJ, Perkinton MS (2009) Synaptic NMDA receptor activation stimulates alpha-secretase amyloid precursor protein processing and inhibits amyloid-beta production. *J Neurosci* 29: 4442 – 4460

Holsinger RM, McLean CA, Beyreuther K, Masters CL, Evin G (2002) Increased expression of the amyloid precursor beta-secretase in Alzheimer's disease. *Ann Neurol* 51: 783 – 786

Holtmaat A, Bonhoeffer T, Chow DK, Chuckowree J, De Paola V, Hofer SB, Hubener M, Keck T, Knott G, Lee WC, Mostany R, Mrsic-Flogel TD, Nedivi E, Portera-Cailliau C, Svoboda K, Trachtenberg JT, Wilbrecht L (2009) Long-term, high-resolution imaging in the mouse neocortex through a chronic cranial window. *Nat Protoc* 4: 1128 – 1144

Jackson KL, Dayton RD, Deverman BE, Klein RL (2016) Better targeting, better efficiency for wide-scale neuronal transduction with the synapsin promoter and AAV-PHP.B. *Front Mol Neurosci* 9: 116

Ji D, Lape R, Dani JA (2001) Timing and location of nicotinic activity enhances or depresses hippocampal synaptic plasticity. *Neuron* 31: 131 – 141

Kamenetz F, Tomita T, Hsieh H, Seabrook G, Borchelt D, Iwatsubo T, Sisodia S, Malinow R (2003) APP processing and synaptic function. *Neuron* 37: 925 – 937

Kendel Y, Melaun C, Kurz A, Nicke A, Peigneur S, Tytgat J, Wunder C, Mebs D, Kauferstein S (2013) Venomous secretions from marine snails of the Terebridae family target acetylcholine receptors. *Toxins (Basel)* 5: 1043 – 1050

Kim M, Suh J, Romano D, Truong MH, Mullin K, Hooli B, Norton D, Tesco G, Elliott K, Wagner SL, Moir RD, Becker KD, Tanzi RE (2009) Potential late-onset Alzheimer's disease-associated mutations in the ADAM10 gene attenuate {alpha}-secretase activity. *Hum Mol Genet* 18: 3987 – 3996

Klevanski M, Saar M, Baumkotter F, Weyer SW, Kins S, Muller UC (2014) Differential role of APP and APLPs for neuromuscular synaptic morphology and function. *Mol Cell Neurosci* 61C: 201 – 210

von Koch CS, Zheng H, Chen H, Trumbauer M, Thinakaran G, van der Ploeg LH, Price DL, Sisodia SS (1997) Generation of APLP2 KO mice and early postnatal lethality in APLP2/APP double KO mice. *Neurobiol Aging* 18: 661 – 669

Korte M, Schmitz D (2016) Cellular and system biology of memory: timing, molecules, and beyond. *Physiol Rev* 96: 647 – 693

Laird FM, Cai H, Savonenko AV, Farah MH, He K, Melnikova T, Wen H, Chiang HC, Xu G, Koliatsos VE, Borchelt DR, Price DL, Lee HK, Wong PC (2005) BACE1, a major determinant of selective vulnerability of the brain to amyloid-beta amyloidogenesis, is essential for cognitive, emotional, and synaptic functions. *J Neurosci* 25: 11693 – 11709

Lannfelt L, Basun H, Wahlund LO, Rowe BA, Wagner SL (1995) Decreased alpha-secretase-cleaved amyloid precursor protein as a diagnostic marker for Alzheimer's disease. *Nat Med* 1: 829 – 832

Laube B, Hirai H, Sturgess M, Betz H, Kuhse J (1997) Molecular determinants of agonist discrimination by NMDA receptor subunits: analysis of the glutamate binding site on the NR2B subunit. *Neuron* 18: 493 – 503

Laube B, Kuhse J, Betz H (1998) Evidence for a tetrameric structure of recombinant NMDA receptors. *J Neurosci* 18: 2954 – 2961

Laube B, Kuhse J, Betz H (2000) Kinetic and mutational analysis of Zn(2+) modulation of recombinant human inhibitory glycine receptors. *J Physiol* 522: 215 – 230

Lawrence JL, Tong M, Alfulaij N, Sherrin T, Contarino M, White MM, Bellinger FP, Todorovic C, Nichols RA (2014) Regulation of presynaptic Ca^{2+}, synaptic plasticity and contextual fear conditioning by a N-terminal beta-amyloid fragment. *J Neurosci* 34: 14210 – 14218

Lazarevic V, Fienko S, Andres-Alonso M, Anni D, Ivanova D, Montenegro-Venegas C, Gundelfinger ED, Cousin MA, Fejtova A (2017) Physiological concentrations of amyloid beta regulate recycling of synaptic vesicles via alpha7 acetylcholine receptor and CDK5/calcineurin signaling. *Front Mol Neurosci* 10: 221

Lee KJ, Moussa CE, Lee Y, Sung Y, Howell BW, Turner RS, Pak DT, Hoe HS (2010) Beta amyloid-independent role of amyloid precursor protein in generation and maintenance of dendritic spines. *Neuroscience* 169: 344 – 356

Li H, Wang B, Wang Z, Guo Q, Tabuchi K, Hammer RE, Sudhof TC, Zheng H (2010) Soluble amyloid precursor protein (APP) regulates transthyretin and Klotho gene expression without rescuing the essential function of APP. *Proc Natl Acad Sci USA* 107: 17362 – 17367

Lipp HP, Wolfer DP (1998) Genetically modified mice and cognition. *Curr Opin Neurobiol* 8: 272 – 280

Ludewig S, Korte M (2016) Novel insights into the physiological function of the APP (Gene) family and its proteolytic fragments in synaptic plasticity. *Front Mol Neurosci* 9: 161

McKay BE, Placzek AN, Dani JA (2007) Regulation of synaptic transmission and plasticity by neuronal nicotinic acetylcholine receptors. *Biochem Pharmacol* 74: 1120 – 1133

Meziane H, Dodart JC, Mathis C, Little S, Clemens J, Paul SM, Ungerer A (1998) Memory-enhancing effects of secreted forms of the beta-amyloid precursor protein in normal and amnestic mice. *Proc Natl Acad Sci USA* 95: 12683 – 12688

Midthune B, Tyan SH, Walsh JJ, Sarsoza F, Eggert S, Hof PR, Dickstein DL, Koo EH (2012) Deletion of the amyloid precursor-like protein 2 (APLP2) does not affect hippocampal neuron morphology or function. *Mol Cell Neurosci* 49: 448 – 455

Mills J, Reiner PB (1999) Mitogen-activated protein kinase is involved in N-methyl-D-aspartate receptor regulation of amyloid precursor protein cleavage. *Neuroscience* 94: 1333 – 1338

Milosch N, Tanriover G, Kundu A, Rami A, Francois JC, Baumkotter F, Weyer SW, Samanta A, Jaschke A, Brod F, Buchholz CJ, Kins S, Behl C, Muller UC, Kogel D (2014) Holo-APP and G-protein-mediated signaling are required for sAPPalpha-induced activation of the Akt survival pathway. *Cell Death Dis* 5: e1391

Mockett BG, Richter M, Abraham WC, Muller UC (2017) Therapeutic potential of secreted amyloid precursor protein APPsalpha. *Front Mol Neurosci* 10: 30

Moreno L, Rose C, Mohanraj A, Allinquant B, Billard JM, Dutar P (2015) sAbetaPPalpha improves hippocampal NMDA-dependent functional alterations linked to healthy aging. *J Alzheimers Dis* 48: 927 – 935

Morris RG, Garrud P, Rawlins JN, O'Keefe J (1982) Place navigation impaired in rats with hippocampal lesions. *Nature* 297: 681 – 683

Müller UC, Deller T, Korte M (2017) Not just amyloid: physiological functions of the amyloid precursor protein family. *Nat Rev Neurosci* 18: 281 – 298

Nikolaev A, McLaughlin T, O'Leary DD, Tessier-Lavigne M (2009) APP binds DR6 to trigger axon pruning and neuron death via distinct caspases. *Nature* 457: 981 – 989

Obregon D, Hou H, Deng J, Giunta B, Tian J, Darlington D, Shahaduzzaman M, Zhu Y, Mori T, Mattson MP, Tan J (2012) Soluble amyloid precursor protein-alpha modulates beta-secretase activity and amyloid-beta generation. *Nat Commun* 3: 777

Olsen O, Kallop DY, McLaughlin T, Huntwork-Rodriguez S, Wu Z, Duggan CD, Simon DJ, Lu Y, Easley-Neal C, Takeda K, Hass PE, Jaworski A, O'Leary DD, Weimer RM, Tessier-Lavigne M (2014) Genetic analysis reveals that amyloid precursor protein and death receptor 6 function in the same pathway to control axonal pruning independent of beta-secretase. *J Neurosci* 34: 6438 – 6447

Olsson A, Hoglund K, Sjogren M, Andreasen N, Minthon L, Lannfelt L, Buerger K, Moller HJ, Hampel H, Davidsson P, Blennow K (2003) Measurement of alpha- and beta-secretase cleaved amyloid precursor protein in cerebrospinal fluid from Alzheimer patients. *Exp Neurol* 183: 74 – 80

Perneczky R, Tsolakidou A, Arnold A, Diehl-Schmid J, Grimmer T, Forstl H, Kurz A, Alexopoulos P (2011) CSF soluble amyloid precursor proteins in the diagnosis of incipient Alzheimer disease. *Neurology* 77: 35 – 38

Perneczky R, Guo LH, Kagerbauer SM, Werle L, Kurz A, Martin J, Alexopoulos P (2013) Soluble amyloid precursor protein beta as blood-based biomarker of Alzheimer's disease. *Transl Psychiat* 3: e227

Peters-Libeu C, Campagna J, Mitsumori M, Poksay KS, Spilman P, Sabogal A, Bredesen DE, John V (2015) sAbetaPPalpha is a potent endogenous inhibitor of BACE1. *J Alzheimers Dis* 47: 545 – 555

Plummer S, Van den Heuvel C, Thornton E, Corrigan F, Cappai R (2016) The neuroprotective properties of the amyloid precursor protein following traumatic brain injury. *Aging Dis* 7: 163 – 179

Puzzo D, Privitera L, Leznik E, Fa M, Staniszewski A, Palmeri A, Arancio O (2008) Picomolar amyloid-beta positively modulates synaptic plasticity and memory in hippocampus. *J Neurosci* 28: 14537 – 14545

Puzzo D, Privitera L, Fa M, Staniszewski A, Hashimoto G, Aziz F, Sakurai M, Ribe EM, Troy CM, Mercken M, Jung SS, Palmeri A, Arancio O (2011) Endogenous amyloid-beta is necessary for hippocampal synaptic plasticity and memory. *Ann Neurol* 69: 819 – 830

Ring S, Weyer SW, Kilian SB, Waldron E, Pietrzik CU, Filippov MA, Herms J, Buchholz C, Eckman CB, Korte M, Wolfer DP, Muller UC (2007) The secreted beta-amyloid precursor protein ectodomain APPs alpha is sufficient to rescue the anatomical, behavioral, and electrophysiological abnormalities of APP-deficient mice. *J Neurosci* 27: 7817 – 7826

Rosen C, Andreasson U, Mattsson N, Marcusson J, Minthon L, Andreasen N, Blennow K, Zetterberg H (2012) Cerebrospinal fluid profiles of amyloid beta-related biomarkers in Alzheimer's disease. *NeuroMol Med* 14: 65 – 73

Saftig P, Lichtenthaler SF (2015) The alpha secretase ADAM10: a metalloprotease with multiple functions in the brain. *Prog Neurobiol* 135: 1 – 20

Seabrook GR, Smith DW, Bowery BJ, Easter A, Reynolds T, Fitzjohn SM, Morton RA, Zheng H, Dawson GR, Sirinathsinghji DJ, Davies CH, Collingridge GL, Hill RG (1999) Mechanisms contributing to the deficits in hippocampal synaptic plasticity in mice lacking amyloid precursor protein. *Neuropharmacology* 38: 349 – 359

Selkoe DJ, Hardy J (2016) The amyloid hypothesis of Alzheimer's disease at 25 years. *EMBO Mol Med* 8: 595 – 608

Sennvik K, Fastbom J, Blomberg M, Wahlund LO, Winblad B, Benedikz E (2000) Levels of alpha- and beta-secretase cleaved amyloid precursor protein in the cerebrospinal fluid of Alzheimer's disease patients. *Neurosci Lett* 278: 169 – 172

Shankar GM, Bloodgood BL, Townsend M, Walsh DM, Selkoe DJ, Sabatini BL (2007) Natural oligomers of the Alzheimer amyloid-beta protein induce reversible synapse loss by modulating an NMDA-type glutamate receptor-dependent signaling pathway. *J Neurosci* 27: 2866 – 2875

Strange BA, Witter MP, Lein ES, Moser EI (2014) Functional organization of the hippocampal longitudinal axis. *Nat Rev Neurosci* 15: 655 – 669

Suh J, Choi SH, Romano DM, Gannon MA, Lesinski AN, Kim DY, Tanzi RE (2013) ADAM10 missense mutations potentiate beta-amyloid accumulation by impairing prodomain chaperone function. *Neuron* 80: 385 – 401

Taylor CJ, Ireland DR, Ballagh I, Bourne K, Marechal NM, Turner PR, Bilkey DK, Tate WP, Abraham WC (2008) Endogenous secreted amyloid precursor protein-alpha regulates hippocampal NMDA receptor function, long-term potentiation and spatial memory. *Neurobiol Dis* 31: 250 – 260

Tyan SH, Shih AY, Walsh JJ, Maruyama H, Sarsoza F, Ku L, Eggert S, Hof PR, Koo EH, Dickstein DL (2012) Amyloid precursor protein (APP) regulates synaptic structure and function. *Mol Cell Neurosci* 51: 43 – 52

Van Nostrand WE, Wagner SL, Shankle WR, Farrow JS, Dick M, Rozemuller JM, Kuiper MA, Wolters EC, Zimmerman J, Cotman CW, Cunningham DD

(1992) Decreased levels of soluble amyloid beta-protein precursor in cerebrospinal fluid of live Alzheimer disease patients. *Proc Natl Acad Sci USA* 89: 2551 – 2555

Vassar R, Kuhn PH, Haass C, Kennedy ME, Rajendran L, Wong PC, Lichtenthaler SF (2014) Function, therapeutic potential and cell biology of BACE proteases: current status and future prospects. *J Neurochem* 130: 4 – 28

Vorhees CV, Williams MT (2014) Assessing spatial learning and memory in rodents. *ILAR J* 55: 310 – 332

Wang P, Yang G, Mosier DR, Chang P, Zaidi T, Gong YD, Zhao NM, Dominguez B, Lee KF, Gan WB, Zheng H (2005) Defective neuromuscular synapses in mice lacking amyloid precursor protein (APP) and APP-Like protein 2. *J Neurosci* 25: 1219 – 1225

Weyer SW, Klevanski M, Delekate A, Voikar V, Aydin D, Hick M, Filippov M, Drost N, Schaller KL, Saar M, Vogt MA, Gass P, Samanta A, Jaschke A, Korte M, Wolfer DP, Caldwell JH, Muller UC (2011) APP and APLP2 are essential at PNS and CNS synapses for transmission, spatial learning and LTP. *EMBO J* 30: 2266 – 2280

Weyer SW, Zagrebelsky M, Herrmann U, Hick M, Ganss L, Gobbert J, Gruber M, Altmann C, Korte M, Deller T, Muller UC (2014) Comparative analysis of single and combined APP/APLP knockouts reveals reduced spine density in APP-KO mice that is prevented by APPsalpha expression. *Acta Neuropathol Commun* 2: 36

Wolfer DP, Madani R, Valenti P, Lipp HP (2001) Extended analysis of path data from mutant mice using the public domain software Wintrack. *Physiol Behav* 73: 745 – 753

Woolley DG, Laeremans A, Gantois I, Mantini D, Vermaercke B, Op de Beeck HP, Swinnen SP, Wenderoth N, Arckens L, D'Hooge R (2013) Homologous involvement of striatum and prefrontal cortex in rodent and human water maze learning. *Proc Natl Acad Sci USA* 110: 3131 – 3136

Xiong M, Jones OD, Peppercorn K, Ohline SM, Tate WP, Abraham WC (2016) Secreted amyloid precursor protein-alpha can restore novel object location memory and hippocampal LTP in aged rats. *Neurobiol Learn Mem* 138: 291 – 299

Yakel JL (2014) Nicotinic ACh receptors in the hippocampal circuit; functional expression and role in synaptic plasticity. *J Physiol* 592: 4147 – 4153

Yan R, Vassar R (2014) Targeting the beta secretase BACE1 for Alzheimer's disease therapy. *Lancet Neurol* 13: 319 – 329

Zou C, Crux S, Marinesco S, Montagna E, Sgobio C, Shi Y, Shi S, Zhu K, Dorostkar MM, Muller UC, Herms J (2016) Amyloid precursor protein maintains constitutive and adaptive plasticity of dendritic spines in adult brain by regulating D-serine homeostasis. *EMBO J* 35: 2213 – 2222